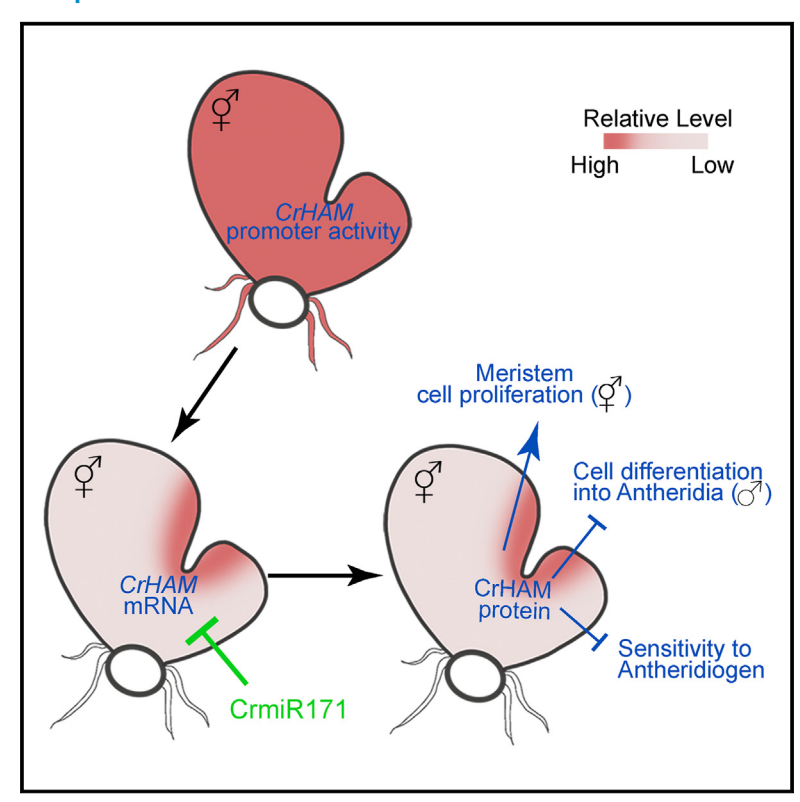
Current Biology

A conserved GRAS-domain transcriptional regulator links meristem indeterminacy to sex determination in Ceratopteris gametophytes

Graphical abstract



Authors

Yuan Geng, Chong Xie, An Yan, Xi Yang, Dinh Nhan Lai, Xing Liu, Yun Zhou

Correspondence

zhouyun@purdue.edu

In brief

The homosporous fern Ceratopteris develops two sex types during the haploid gametophyte phase: the meristem-containing hermaphrodite and the ameristic male. Geng et al. find that the GRAS protein CrHAM maintains hermaphrodite identity and development by sustaining meristem cell proliferation and repressing the male differentiation program.

Highlights

- CrHAM differentially accumulates in Ceratopteris hermaphrodites and males
- CrHAM maintains meristem indeterminacy and cell division in hermaphrodites
- CrHAM suppresses antheridiogen-mediated male differentiation, affecting sex ratio
- miR171 represses CrHAM during gametophyte development in Ceratopteris



Current Biology



Article

A conserved GRAS-domain transcriptional regulator links meristem indeterminacy to sex determination in Ceratopteris gametophytes

Yuan Geng,^{1,2,6,7} Chong Xie,^{1,2,7} An Yan,^{3,4} Xi Yang,^{1,2} Dinh Nhan Lai,^{1,2} Xing Liu,^{2,5} and Yun Zhou^{1,2,8,*}

SUMMARY

Most land plants alternate between generations of sexual gametophytes and asexual sporophytes. Unlike seed plants, fern gametophytes are free living and grow independently of their sporophytes. In homosporous ferns such as Ceratopteris, gametophytes derived from genetically identical spores exhibit sexual dimorphism, developing as either males or hermaphrodites. Males lack meristems and promote cell differentiation into sperm-producing antheridia. In contrast, hermaphrodites initiate multicellular meristems that stay undifferentiated, sustain cell division and prothallus expansion, and drive the formation of egg-producing archegonia. Once initiating the meristem, hermaphrodites secrete the pheromone antheridiogen, which triggers neighboring slower-growing gametophytes to develop as males, while the hermaphrodites themselves remain insensitive to antheridiogen. This strategy promotes outcrossing and prevents all individuals in the colony from becoming males. This study reveals that an evolutionarily conserved GRAS-domain transcriptional regulator (CrHAM), directly repressed by Ceratopteris microRNA171 (CrmiR171), promotes meristem development in Ceratopteris gametophytes and determines the male-to-hermaphrodite ratio in the colony. CrHAM preferentially accumulates within the meristems of hermaphrodites but is excluded from differentiated antheridia. CrHAM sustains meristem proliferation and cell division through conserved hormone pathways. In the meantime, CrHAM inhibits the antheridiogen-induced conversion of hermaphrodites to males by suppressing the male program expression and preventing meristem cells from differentiating into sperm-producing antheridia. This finding establishes a connection between meristem indeterminacy and sex determination in ferns, suggesting both conserved and diversified roles of meristem regulators in land plants.

INTRODUCTION

Meristems in land plants share conserved and essential roles in sustaining cell proliferation, driving organ formation, and determining body architectures. ^{1–3} Different from the gametophytes (the haploid sexual phase) in seed plants, which are dependent on their sporophytes (the diploid asexual phase) and are devoid of any meristem, ^{4,5} fern gametophytes grow independently of their sporophytes and maintain pluripotent meristems to sustain prothallus expansion and sexual organ formation (Figure S1A). ^{6–8} Over the last 30 years, the fern *Ceratopteris richardii* (hereafter referred to as Ceratopteris) has been developed as an efficient model system to study gametophytes of homosporous ferns, including their physiology, evolution, and developmental processes. ^{6,9–21} Under the influence of antheridiogen (a pheromone), Ceratopteris gametophytes germinating from genetically identical

spores exhibit sexual dimorphism, with either male or hermaphroditic sex (Figure S1A). 6,20 Male gametophytes (males) do not contain meristems, and their cells quickly enter differentiation to form a number of sperm-producing antheridia, which is the male trait. In contrast, hermaphroditic gametophytes (hermaphrodites) develop the multicellular meristem and egg-producing archegonia, both of which are the female traits, and a few antheridia, the male trait. 6,20,22 The multicellular meristem in hermaphrodites stays undifferentiated and sustains cell division, eventually resulting in an expanded, cordate prothallus with an iconic meristem notch at the center. 12,20,22 One previous study, combining longterm time-lapse confocal imaging and computational analysis in Ceratopteris hermaphrodites, uncovered cell division dynamics of multicellular meristems, quantitatively determining division activity and reconstructing cell lineages during meristem formation and proliferation.²² However, the molecular mechanisms

¹Department of Botany and Plant Pathology, Purdue University, West Lafayette, IN 47907, USA

²Purdue Center for Plant Biology, Purdue University, West Lafayette, IN 47907, USA

³Division of Biology and Biological Engineering, California Institute of Technology, Pasadena, CA 91125, USA

⁴Howard Hughes Medical Institute, California Institute of Technology, Pasadena, CA 91125, USA

⁵Department of Biochemistry, Purdue University, West Lafayette, IN 47907, USA

⁶Present address: Division of Chemistry and Chemical Engineering, California Institute of Technology, Pasadena, CA 91125, USA

⁷These authors contributed equally

⁸Lead contact

^{*}Correspondence: zhouyun@purdue.edu https://doi.org/10.1016/j.cub.2024.06.064





underlying meristem initiation and maintenance in Ceratopteris gametophytes are still largely unresolved.

The fact that Ceratopteris hermaphrodites always develop and maintain a multicellular meristem, while males are exclusively ameristic (lacking any meristem),²⁰ suggests yet-undefined mechanisms connecting sex types to meristem development in Ceratopteris gametophytes. In a colony of Ceratopteris spores, an early-germinated spore develops as a hermaphrodite. 6,20,22 Once it initiates a multicellular meristem, the hermaphrodite secretes antheridiogen into its surroundings, triggering the neighboring slower-growing gametophytes to become males.^{6,20} Meanwhile, the hermaphrodite maintains itself insensitive to antheridiogen, continuously promoting prothallus expansion and eventually producing egg-forming archegonia for fertilization.²⁰ This strategy promotes outcrossing, increases genetic diversity, and prevents the entire colony from becoming exclusively males. Multiple Ceratopteris mutants affecting sex determination in gametophytes have been isolated and characterized. 11 For example, the transformer (tra) and hermaphroditic (her) mutants develop exclusively as males and hermaphrodites, respectively, regardless of the absence or presence of antheridiogen (A_{CE}, antheridiogen from Ceratopteris). 23,24 Due to the large size and high complexity of the Ceratopteris genome, the causal mutations still remain to be identified, 11,25,26 and thus, the molecular components in the pathway are unclear. Furthermore, it remains puzzling why the meristem-containing hermaphrodites are insensitive to antheridiogen, thereby maintaining their meristem activity and hermaphroditic identity.

We wonder whether the conserved regulatory machinery is shared between the multicellular meristems in Ceratopteris gametophytes and the apical meristems (such as shoot apical meristems, SAMs) in sporophytes of seed plants. The HAIRY MERI-STEM (HAM, also known as LOST MERISTEMS, LOMs²⁷) family GRAS-domain transcriptional regulators are widely present in multiple lineages of land plants. 28,29 In several seed plants, including the model organism Arabidopsis, HAM family members play essential roles in maintaining the indeterminacy and proliferation of stem cells within the SAMs. 27,30-37 Mutations in HAM genes lead to abnormal meristem morphology, early termination of SAMs, and even the differentiation of meristematic cells into trichome-like structures. 27,32-37 Cross-species complementation assays have demonstrated that different HAM members from seed plants or seed-free plants share conserved functions with the Arabidopsis type II HAM genes (AtHAM1-3) in maintaining the identity of established SAMs, shaping the expression patterns of downstream genes, and promoting the initiation of axillary meristems in Arabidopsis.²⁸ In addition, microRNA171 (miR171) specifically recognizes and cleaves the transcripts of AtHAM1-3, which defines an apical-basal expression gradient of HAM proteins in Arabidopsis SAMs. 32,38-41 Importantly, the 21-nt miR171 binding sites are highly conserved across the HAM members from seed-free plant lineages and the type II HAM genes from seed plants.^{28,29} Through transcriptomic studies and phylogenetic analysis, we identified a HAM homolog in Ceratopteris (CrHAM), 9,28,42 which is expressed in both gametophytes and sporophytes.9 Interestingly, the miR171 binding site within the CrHAM coding sequence is identical to that in the Arabidopsis HAM1-3 genes.²⁸ All the knowledge gained from the previous studies suggested that CrHAM, along with its potential negative

regulator (miR171), presents promising candidates for exploring the mechanism underlying meristem development in Ceratopteris hermaphrodites.

In this work, we performed transgenic studies, confocal live imaging, and phylogenetic analysis in Ceratopteris, and we analyzed dynamic transcriptomic profiles of Ceratopteris gametophytes. Our findings demonstrate the specific accumulation of the CrHAM protein in the meristem during Ceratopteris hermaphrodite development. Notably, CrHAM plays a crucial role in maintaining meristem identity and inhibiting the antheridiogeninduced conversion from hermaphrodites to males. Specifically, CrHAM, which is negatively regulated by CrmiR171, promotes cell division and prevents meristem cells from differentiating into sperm-producing antheridia. This discovery establishes a vital connection between meristem indeterminacy and sex determination in Ceratopteris gametophytes.

RESULTS

CrHAM is highly expressed in undifferentiated meristems in hermaphrodites but excluded from differentiated antheridia in males

We first examined the expression patterns of the CrHAM gene during the gametophyte stage using quantitative PCR (qPCR) analysis. Seven days after the wild-type (WT) Ceratopteris spores were germinated, we identified and separately collected hermaphrodites and males for RNA isolation. The data showed that hermaphrodites accumulated significantly more CrHAM transcripts compared with ameristic males (Figure 1A). For a more detailed examination of the spatiotemporal patterns of CrHAM in Ceratopteris hermaphrodites and males, we generated and characterized multiple independent transgenic lines of two different fluorescent reporters: the established miR171-insensitive CrHAM transcriptional reporter (pCrHAM::H2B-GFP::3'CrHAM)²² and the new miR171-sensitive CrHAM translational reporter (pCrHAM::YPET-CrHAM::3'CrHAM) (Figures 1B and 1C). In the pCrHAM::H2B-GFP::3'CrHAM reporter, the Histone 2B (H2B)-GFP fusion fragment^{22,39} was expressed under the control of the 2.3-kb endogenous 5' promoter and the 1.0-kb 3' terminator/untranslated region from CrHAM, thereby reflecting the promoter activity of CrHAM (Figure 1B).²² Subsequently, we replaced the H2B-GFP coding sequence with the sequence encoding the YPET-CrHAM fusion protein²⁸ to generate the pCrHAM::YPET-CrHAM::3'CrHAM reporter (Figure 1C). The pCrHAM::YPET-CrHAM::3'CrHAM reporter maintains the conserved miR171 binding site (indicated by the arrowhead in Figure 1C) within the CrHAM coding sequence.²⁸ Therefore, it reflected the level and distribution of the CrHAM protein, at least partially, impacted by miR171 activity.

Using laser scanning confocal microscopy, we imaged both reporters in transgenic Ceratopteris gametophytes at various developmental stages (Figures 1D–1S, S1B, and S1C). Consistent with our previous findings, the *pCrHAM::H2B-GFP::3'CrHAM* reporter exhibited ubiquitous expression in the prothalli of both hermaphrodites and males throughout their developmental stages (Figures 1D–1G). The expression was observed in both undifferentiated meristems (indicated by arrows in Figures 1D–1F) and differentiated cells, including those composing developing antheridia (highlighted by dashed circles in Figures 1E



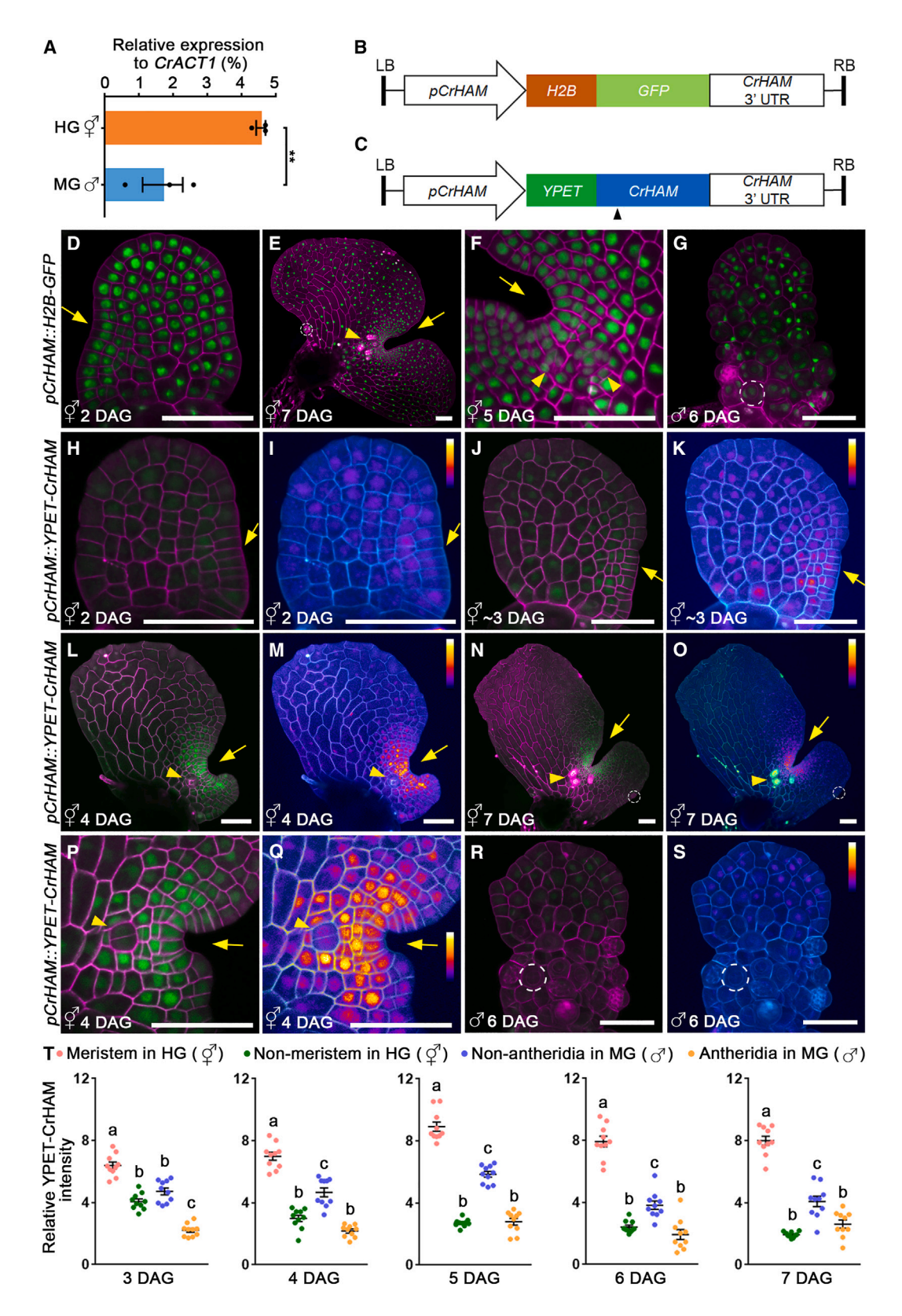


Figure 1. Dynamic expression patterns of CrHAM in Ceratopteris gametophytes

(A) Relative expression of *CrHAM* in WT determined by quantitative PCR (qPCR) analysis, normalized to the reference gene *CrACTIN1* (*CrACT1*). HG, hermaphroditic gametophytes ($\[3\]$); MG, male gametophytes ($\[3\]$). Bars: means \pm standard errors of the mean (SEMs), n=3 biological replicates. **p<0.01 (Student's two-tailed t test).





and 1G).²² In contrast, the pCrHAM::YPET-CrHAM::3'CrHAM translational reporter showed differential expressions during gametophyte development (Figures 1H-1S) as revealed by heatmaps at different days after germination (DAG) (Figures 1I, 1K, 1M, 1O, 1Q, and 1S). The translational reporter showed slightly higher expression in the apical region and the meristem initiation site in young hermaphrodites (Figures 1H-1K). As meristem notches formed in hermaphrodites, the reporter signal gradually and preferentially accumulated in the meristem cells adjacent to the notch (arrows in Figures 1L-1Q), while it greatly decreased in cells located distally to the notch or outside of the meristem (Figures 1L-1Q). Notably, this reporter signal was also excluded from the antheridia developed in hermaphrodites (dashed circles in Figures 1N and 10). Once the multicellular meristem was fully established, the reporter signal was specifically localized to the undifferentiated meristem in hermaphrodites (Figures 1N and 10). We also detected the reporter signal in the apical region of males, where the cells had not differentiated into antheridia yet (Figures 1R and 1S). Overall, the reporter signal was lower in males (Figures 1R and 1S) than in hermaphrodites (Figures 1L-1Q), consistent with the qPCR result (Figure 1A).

We then conducted quantitative image analysis to comprehensively determine the dynamic patterns of the CrHAM protein across different cell types and sex types. We spread spores of the pCrHAM::YPET-CrHAM::3'CrHAM reporter line on fern medium (FM), and we randomly sampled multiple independent gametophytes each day from 3 to 7 DAG. For each sample, we identified the sex type and simultaneously quantified the YPET-CrHAM signals from different functional groups, including meristems in hermaphrodites, non-meristem regions in hermaphrodites, antheridia in males, and non-antheridia regions in males. As illustrated in Figure 1T, our data revealed that high CrHAM levels were positively correlated with meristem initiation and establishment in hermaphrodites (at 3-7 DAG) but negatively correlated with antheridium formation in males during gametophyte development.

CrHAM loss of function leads to the increased male-tohermaphrodite ratio and abnormal hermaphrodite development

We observed the specific and restricted accumulation of the CrHAM protein in Ceratopteris gametophytes (Figure 1). This

promoted us to examine whether the HAM family is involved in meristem development during the gametophyte phase and whether CrHAM contributes to hermaphrodite development in Ceratopteris. In contrast to the four HAM homologs in Arabidopsis, ^{28,34} only one HAM homology (CrHAM) was identified in the Ceratopteris genome, allowing us to study the HAM function without the influence of functional redundancy. However, if CrHAM is crucial for gametophyte formation and sexual reproduction, recovering its null mutant could be potentially challenging. With this consideration, we generated transgenic Ceratopteris plants with CrHAM knockdown (CrHAM KD) to achieve partial loss of function. Specifically, the RNA interference (RNAi) hairpin-forming expression cassette that targets CrHAM was cloned in pANDA35HK43 (Figure S2A) and stably transformed into Ceratopteris. More than ten independent transgenic lines were obtained and, among them, three lines (lines 37, 111, and 251) exhibited significantly reduced expression of CrHAM compared with that in the WT control (Figure S2B).

When growing these three CrHAM KD lines on FM, we observed that more gametophytes developed as males. In addition, at the same DAG, while the morphology of CrHAM KD males was similar to that of the WT control, CrHAM KD hermaphrodites exhibited abnormal morphology compared with the WT (Figures 2A-2E). We then performed a quantitative assay to determine the sex ratios and to characterize gametophyte morphology in both the WT and CrHAM KD populations (Figure 2F). Specifically, spores of the WT and CrHAM KD were surface-sterilized and spread on FM in petri dishes at a similar density (to exclude the potential effect of population density on the sex ratio²⁵) and were cultured under identical conditions. At 4-6 DAG, when hermaphrodites and males were morphologically distinguishable, five 1-cm² squares were randomly selected from the FM (Figure 2F), and all the gametophytes, WT, or CrHAM KD, grown in each selected area were stained with propidium iodide and imaged through confocal microscopy (Data S1). Based on the confocal images (Data S1), each gametophyte was unambiguously identified as a hermaphrodite or an ameristic male, and the sex ratios of the gametophyte populations were then determined per genotype (Figure 2G). In WT gametophytes, 70.5% developed as hermaphrodites and 29.5% as males (Figure 2G). In contrast, in the CrHAM KD populations with sample sizes comparable to that of WT, a reduction in the number of

(B and C) Schematic diagrams showing the expression cassettes of the CrHAM transcriptional reporter pCrHAM::H2B-GFP::3'CrHAM (B) and the translational reporter pCrHAM::YPET-CrHAM::3'CrHAM (C). pCrHAM, the CrHAM endogenous promoter; H2B, histone 2B; GFP, green fluorescent protein; CrHAM 3'UTR, the endogenous 3' untranslated region/terminator of the CrHAM gene; YPET, yellow fluorescent protein. Black arrowhead, the conserved microRNA171 binding site: LB. left border: RB. right border.

(D-G) Z-projection views of confocal images showing gametophytes of the pCrHAM::H2B-GFP::3'CrHAM transgenic reporter line at different days after germination (DAG).

(F) A close-up view of a multicellular meristem and surrounding developing archegonia.

(H–S) Z-projection views of confocal images showing gametophytes of the pCrHAM::YPET-CrHAM transgenic reporter line at different DAG. (P and Q) A close-up view of a multicellular meristem and a subtending developing archegonium. (D-G) Merged GFP (green) and propidium iodide (PI) counterstain (magenta, showing the cell outline).

(H, J, L, N, P, and R) Merged YPET (green) and PI (magenta).

(I, K, M, O, Q, and S) Heatmaps of YPET (fire LUT, look up tables) with PI counterstain. Scale bars, 100 µm. Color bars (I, K, M, O, Q, and S): fire LUT. Yellow arrows, meristems; yellow arrowheads, archegonia; white circles, antheridia.

(T) Relative fluorescence signal (YPET-CrHAM) intensity from different functional regions: meristems in HG (otin), non-meristem regions in HG (otin), antheridia in MG (3), and non-antheridia regions in MG (3). Differences between each two groups were determined by one-way ANOVA, followed by Tukey's test. Values not sharing a common letter indicate significant differences (p < 0.05, n = 10). See also Figure S1.



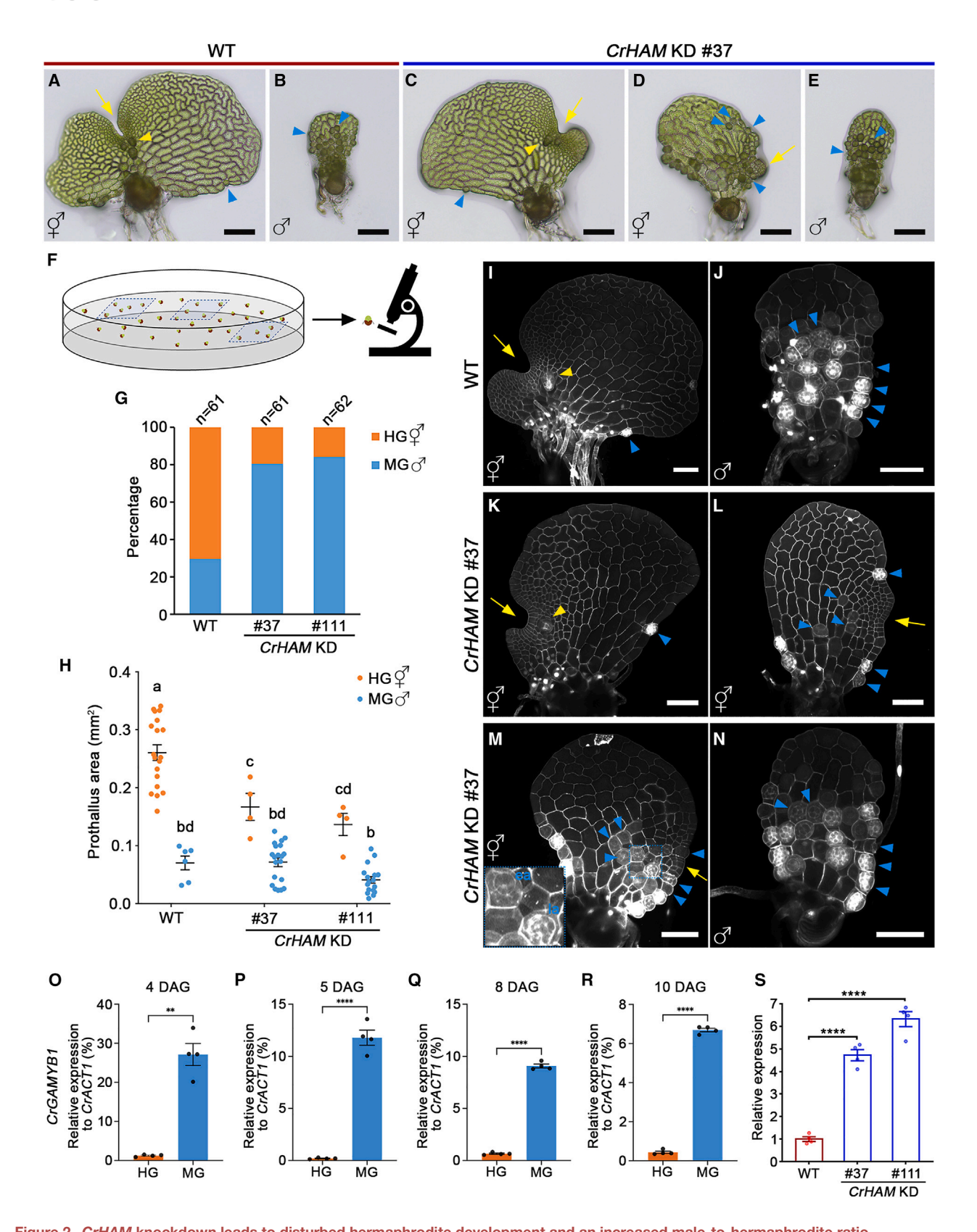


Figure 2. CrHAM knockdown leads to disturbed hermaphrodite development and an increased male-to-hermaphrodite ratio (A–E) Light micrographs of gametophytes from the wild-type (WT) control (A and B) and one representative CrHAM knockdown (CrHAM KD) transgenic line (line 37) (C–E) at 6 DAG.





hermaphrodites and an increase in the number of males was observed, resulting in an increased male-to-hermaphrodite ratio (Figure 2G; Data S1). Only ~20% of CrHAM KD gametophytes were hermaphrodites, and a much larger proportion (~80%) developed as males (Figure 2G). We then quantified the prothallus (gametophyte) size (Figure 2H), which has been demonstrated as one quantitative trait for sex types and gametophyte development: Ceratopteris hermaphrodites have expanded prothalli because they maintain the multicellular meristem and sustain cell proliferation, whereas ameristic males have much smaller prothalli. 6,20 Our quantification results showed that, at 4 DAG, the average prothallus size of CrHAM KD males was comparable to the WT (Figure 2H). However, the average prothallus size of CrHAM KD hermaphrodites was significantly smaller than that of the WT (Figure 2H). The same confocal images also allowed us to examine the anatomy and morphology of hermaphrodites and males at high resolution (Figures 2I-2N; Data S1). The morphology of these WT gametophytes examined here was consistent with the characterizations in the previous reports.^{20,22} When grown on FM plates, WT hermaphrodites established a multicellular meristem and formed a few archegonia beneath the meristem notch (Figure 2I; Data S1). A few antheridia were formed on these WT hermaphrodites, which always initiated distally to the meristem notch (Figure 2I; Data S1). WT males lack a multicellular meristem, and the majority of cells in the basal region of the prothalli differentiated into sperm-producing antheridia (Figure 2J; Data S1). Interestingly, in CrHAM KD hermaphrodites, the multicellular meristem was generally reduced in size compared with the WT (Figures 2I, 2K, and 2L; Data S1), showing a much shallower notch at the same DAG. Furthermore, in multiple gametophytes, no or few archegonia were observed surrounding the abnormal CrHAM KD meristem (Figures 2L and 2M; Data S1). Instead, a number of antheridia appeared directly surrounding the meristem and even within the meristem region (Figures 2D, 2L, and 2M; Data S1). All these data suggested a role of CrHAM in sex determination, promoting the female traits (meristem development and archegonium formation), and suppressing the male trait (antheridium differentiation).

To explore the mechanism by which CrHAM KD resulted in an increased male-to-hermaphrodite ratio, we cultured WT and

CrHAM KD spores individually in the 48-well tissue culture plates containing FM without or with various concentrations (10%, 50%, and 100%) of exogenous A_{CE}. In the absence of exogenous A_{CE}, all WT and CrHAM KD spores developed as hermaphrodites (Figure S2C), indicating that even in the CrHAM KD background, sensing exogenous A_{CE} was necessary for male programming. Interestingly, compared with the WT, CrHAM KD gametophytes exhibited higher sensitivity to exogenous A_{CE} (Figure S2D). Specifically, when exposed to 10% exogenous A_{CE}, only 49% of WT spores developed into males, suggesting that A_{CE} sensitivity is a quantitative trait in Ceratopteris, and each gametophyte may respond variably to the same low concentration of A_{CE}. In contrast, when exposed to 10% A_{CE}, a striking 94% of individually cultured CrHAM KD spores developed into males, suggesting that CrHAM functions to desensitize the A_{CE} response (Figure S2D). In addition, as shown in Figure 2H, CrHAM KD hermaphrodites generally showed smaller prothallus sizes compared with the WT. This led us to wonder whether the increased male-to-hermaphrodite ratio in the CrHAM KD population was partially due to the slow growth of CrHAM KD hermaphrodites. To test this, we cultured both WT and CrHAM KD gametophytes at a lower temperature (22°C) to slow down overall growth and then compared the percentages of males in each genotype with the same batch of gametophytes cultured under standard growth conditions (at 28°C). Interestingly, at both high and low temperatures, CrHAM KD consistently exhibited a higher male-to-hermaphrodite ratio compared with the WT (Figure S2E), suggesting that the increased male ratio in the CrHAM KD population is not directly related to the smaller size and slower growth of CrHAM KD hermaphrodites.

Upregulation of male-specific *GAMYB* genes in *CrHAM* KD gametophytes

We then investigated molecular markers associated with the CrHAM-mediated repression of male traits. In several flowering plants, the GAMYB family transcription factors, controlled by the gibberellin acid (GA) signaling pathway, plays a crucial role in male gametophyte (pollen) development. ^{44–46} Interestingly, by now, all the characterized antheridiogens in ferns are GAs or their derivatives. ^{47,48} Consequently, it has been proposed

⁽F) Experimental design for determining sex ratios of gametophytes from the WT and CrHAM KD populations. Equal amounts of spores of each genotype were sown on FM plates and cultured under identical conditions. When sex types of gametophytes were distinguishable (4–6 DAG), multiple 1-cm² squares were randomly selected from FM plates, and all gametophytes within each square were stained and imaged using laser scanning confocal microscopy. Each gametophyte was identified as a hermaphrodite with a meristem or an ameristic male (as shown in confocal images in Data S1), and the sex ratio of gametophytes in the corresponding area was determined.

⁽G) Percentages of hermaphroditic gametophytes (HGs) and male gametophytes (MGs) in the gametophyte populations of the WT control (n = 61 gametophytes from five different regions/areas), and the *CrHAM* KD line 37 (n = 61 gametophytes from five different regions/areas), and the *CrHAM* KD line 111 (n = 62 gametophytes from five different regions/areas).

⁽H) Prothallus areas of gametophytes at 4 DAG in the WT and the two *CrHAM* KD lines (37 and 111). Dots represent individual gametophytes, horizontal lines show means, and error bars represent SEMs. Differences between each two groups were determined by one-way ANOVA, followed by Tukey's test. Values not sharing a common letter indicate significant differences (p < 0.05).

⁽I–N) Confocal images of gametophytes at 4 DAG from WT and *CrHAM* KD populations. Gametophytes were identified as hermaphrodites with meristems (I, K, L, and M) or ameristic males (J and N). Insert in (M): a close-up view of an early-stage antheridium (ea) and a late-stage antheridium (la). Gray: PI counterstain. Yellow arrows, meristems; yellow arrowheads, archegonia; blue arrowheads, antheridia. Scale bars, 200 μm (A–E) and 100 μm (I–N).

⁽O–R) Relative expressions of *CrGAMYB1* at different sex types and various developmental stages were determined by qPCR analysis and normalized to *CrACT1*. Samples include WT HG and WT MG at 4 (O), 5 (P), 8 (Q), and 10 (R) DAG.

⁽S) Relative expression levels of CrGAMYB1 in gametophytes at 7 DAG from WT and CrHAM KD populations (normalized to CrACT1). The expression level in CrHAM KD hermaphrodites was normalized to that in WT. Bars: means \pm SEMs, n = 4 biological replicates. **p < 0.001; *****p < 0.0001 (Student's two-tailed t test). See also Figures S2 and S3 and Data S1 and S2.



that the A_{CE}-triggered antheridium formation and male gametophyte development in Ceratopteris share common components (such as GAMYB) with the GA signaling pathway in flowering plants.¹¹ Through homolog search and phylogenetic analysis (Data S2), we identified four GAMYB genes in the Ceratopteris genome, named CrGAMYB1-4. Our expression analysis revealed that three of them - CrGAMYB1, CrGAMYB2, and CrGA-MYB3-are specifically expressed in males at various DAG (Figures 20-2R, S3A-S3D, S3F-S3I, and S3N). These results suggested that the male gametophyte-specific expressions of GAMYB genes are conserved in ferns and flowering plants, and CrGAMYB1-3 serve as specific markers for the male trait in Ceratopteris. Furthermore, we examined the expression levels of CrGAMYB1-3 in the gametophyte populations of the WT and CrHAM KD. All three CrGAMYB genes were significantly upregulated in CrHAM KD gametophytes compared with the WT (Figures 2S, S3E, and S3J). Notably, the upregulation occurred in CrHAM KD gametophytes as early as 3 DAG (Figures S3K-S3M), coinciding with the emergence of morphological differences between hermaphrodites and males. These results align with the observed increase in the male-to-hermaphrodite ratio and the greater number of antheridia in CrHAM KD gametophytes (Figures 2G, 2L, and 2M).

CrHAM suppresses the effects of antheridiogen on meristems of hermaphrodites

Our finding immediately raises a new question: how does the meristem-expressed CrHAM determine the percentage of ameristic males in the gametophyte population (Figure 2G)? Considering the observed ectopic formation of antheridia surrounding the meristem in several CrHAM KD samples (Figures 2D, 2L, and 2M), it is possible that when A_{CE} is released from siblings and sensed by the hermaphrodites, CrHAM KD hermaphrodites cannot maintain their meristems undifferentiated. Consequently, a considerable number of young hermaphrodites gradually convert themselves into ameristic males, resulting in an increased male-to-hermaphrodite ratio. To test this hypothesis, we performed the single-spore assay (Figure 3A; STAR Methods) and individually followed the fate of each gametophyte in response to A_{CE}. In this assay, we inoculated a single spore per well in the 48-well tissue culture plates containing FM (Figure 3A). Hence, the spores were isolated and were not exposed to A_{CE} secreted from neighboring hermaphrodites (Figure 3A). In the absence of exogenous A_{CE}, all the germinated spores developed into hermaphrodites, as previously characterized.²⁰ At 2 DAG, we stained and imaged young hermaphrodites and then transferred the individuals onto the FM plates supplemented with the exogenous $\ensuremath{A_{\text{CE}}}$ $(FM + A_{CE})$ (Figures 3A–3E). Four days after the A_{CE} treatment, we stained and imaged the same gametophytes using confocal microscopy (Figures 3A and 3F-3I). Previous findings showed that once a WT Ceratopteris gametophyte develops into a hermaphrodite, it becomes insensitive to A_{CE}, and its hermaphroditic developmental programming cannot be terminated or reverted to male programming by exposure to exogenous A_{CE}.²⁰ As expected, all WT gametophytes in our assay remained hermaphrodites, forming the meristem notch and archegonia adjacent to the meristem (Figures 3B and 3F; Table S1). None of them (0/17) converted to males (Figure 3J; Table S1). However, when the CrHAM activity was reduced (Figures 3C-3E and 3G-3I), 22%-37% of CrHAM KD hermaphrodites were converted to ameristic males in the presence of exogenous A_{CE} (Figures 3E, 3I, and 3J; Table S1). The remaining CrHAM KD maintained themselves as hermaphrodites with the meristem and archegonia (Figure 3J; Table S1). Among them, the meristems generally reduced in size, and some gametophytes displayed partial termination of meristems, forming many antheridia (indicated by blue arrowheads) instead of archegonia (indicated by yellow arrowheads) surrounding the meristem (Figures 3G and 3H). We further quantified the female and male traits in each imaged gametophyte (Figures 3K and 3L; Table S1). Compared with the WT, the average number of antheridia was significantly increased in the CrHAM KD gametophytes (Figure 3K; Table S1). Conversely, as the key female trait and an indicator of meristem activity, the archegonium number was reduced in CrHAM KD gametophytes (Figure 3L; Table S1). These quantitative data, along with the expression pattern of CrHAM in hermaphrodites, suggest that meristem-expressed CrHAM prevents hermaphrodites from responding to A_{CE}, maintaining meristem indeterminacy and prohibiting the conversion from hermaphrodites to ameristic males.

CrHAM promotes cell proliferation during meristem establishment in hermaphrodites

Thus far, our data (Figures 2, 3, S2, and S3; Data S1) support a working model that CrHAM prevents cells from differentiating into antheridia, suppressing the male trait, and promoting hermaphrodite development. Interestingly, CrHAM KD hermaphrodites generally exhibit smaller prothallus sizes than the WT, regardless of whether they initiate more antheridia surrounding the meristems (Figures 2A, 2C, 2D, 2H, 2I, and 2K-2M; Data S1). These results suggest that CrHAM has additional roles in promoting hermaphrodite development besides inhibiting (antheridium) cell differentiation. Because these roles are independent of the A_{CE} response, we performed a different singlespore assay. Specifically, we cultured each spore individually in wells of 48-well culturing plates containing FM and quantified the growth dynamics of hermaphrodites in the absence of exogenous A_{CE} (Figures 4A-4G). Up to 2 DAG, WT, and CrHAM KD hermaphrodites exhibited similar morphology. At this stage, the size and cell number of CrHAM KD prothalli were comparable to those of the WT control (Figures 4B, 4E, 4H, and 4I). However, starting from 3 DAG, when multicellular meristems began to initiate and establish, WT and CrHAM KD hermaphrodites became different in morphology (Figures 4C, 4D, and 4F-4I). At 5 DAG, compared with the WT control, CrHAM KD hermaphrodites formed a shallower meristem notch, initiated fewer archegonia near the meristem notch, but developed more antheridia near or distal to the meristem notch (Figures 4D and 4G). In addition, the prothallus size and the total cell number per prothallus were significantly decreased in CrHAM KD hermaphrodites (Figures 4H and 4I).

To test whether the smaller prothallus size and lower cell number in *CrHAM* KD hermaphrodites can be attributed to reduced cell division during the early phase of meristem initiation, we quantified division activity in both WT and *CrHAM* KD hermaphrodites (2 DAG). We stained the hermaphrodites with 5-ethynyl-2'-deoxyuridine (EdU), a fluorescent dye incorporated into cells during DNA synthesis and used for detecting dividing cells. ^{49,50} After 3 h of EdU treatment (see details in STAR Methods), we



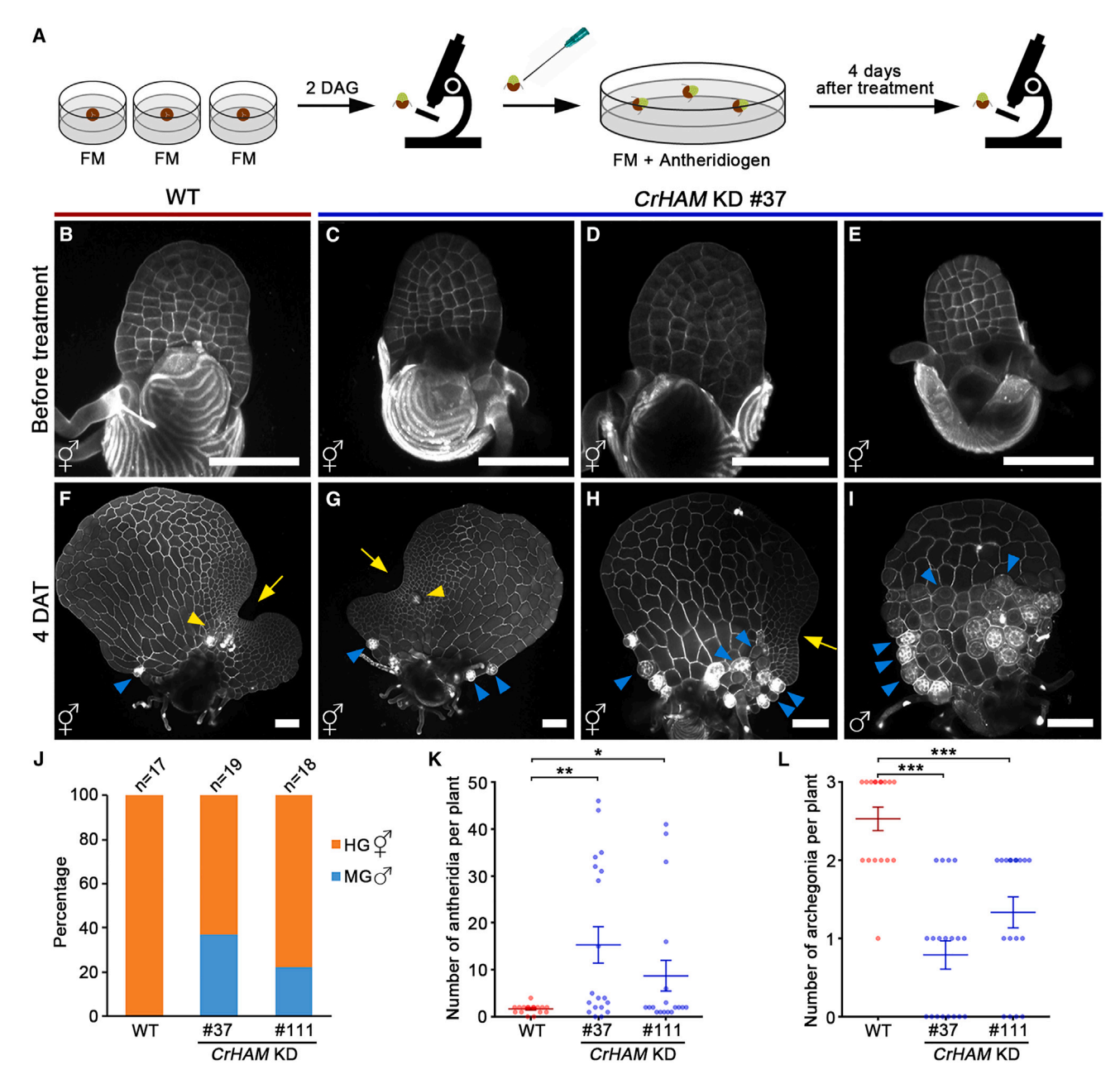


Figure 3. Suppression of CrHAM expression enables the antheridiogen (A_{CE}) response in Ceratopteris hermaphrodites

(A) The experimental design for determining the effects of A_{CE} on hermaphrodite development. A single spore was sown in each individual well containing FM and 0.7% (w/v) agar. In the absence of exogenous A_{CE} , all gametophytes developed as hermaphrodites. At 2 DAG, gametophytes were imaged and transferred to FM plates supplemented with A_{CE} . After 4 days of A_{CE} treatment, the same hermaphrodites were imaged again, and their sex types were identified based on confocal images.

(B–I) Confocal images of the same gametophytes before (B–E) and after the 4-day treatment with exogenous A_{CE} (F–I). The gametophytes shown in (F)–(H) were identified as hermaphrodites, some of which (G and H) developed meristems with reduced sizes. The gametophyte shown in (I) was identified as an ameristic male. Gray: PI counterstain. Yellow arrows, meristems; yellow arrowheads, archegonia; blue arrowheads, antheridia. Scale bars, 100 μ m.

(J) Percentages of hermaphroditic gametophytes (HGs) and male gametophytes (MGs) among gametophytes in different genotypes after A_{CE} treatment. (K and L) Numbers of antheridia (K) and archegonia (L) per gametophyte after A_{CE} treatment in different genotypes.

Samples in (J)–(L) include the WT control (n = 17 biological replicates), CrHAM KD line 37 (n = 19 biological replicates), and CrHAM KD line 111 (n = 18 biological replicates). Dots represent individual gametophytes, horizontal lines show means, and error bars represent SEMs in (K) and (L). *p < 0.05; **p < 0.01; ***p < 0.001 (Student's two-tailed t test).

See also Figure S2 and Table S1.



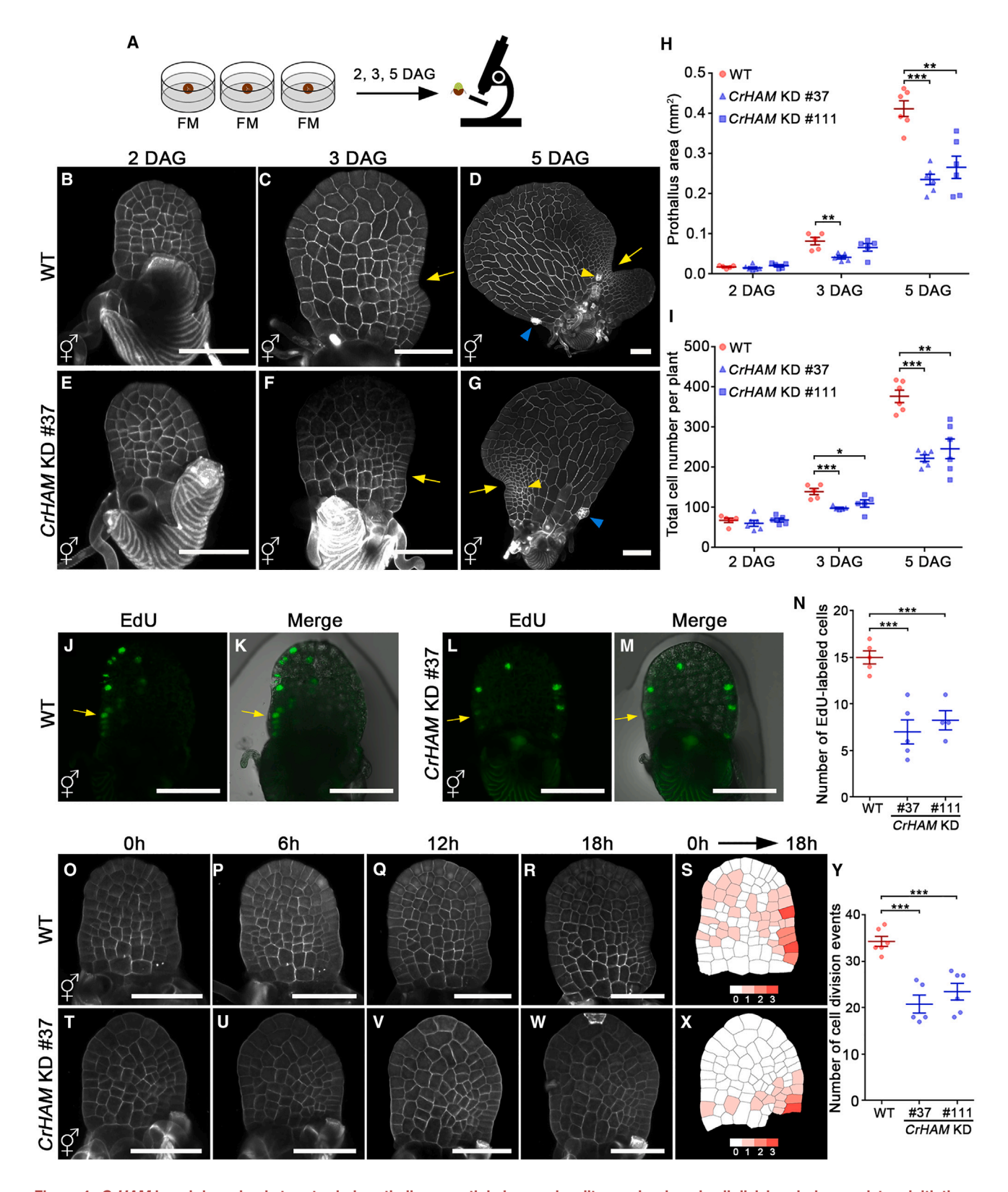


Figure 4. CrHAM knockdown leads to retarded prothallus growth in hermaphrodites and reduced cell division during meristem initiation (A) The experimental design for examining prothallus expansion and cell proliferation in Ceratopteris hermaphrodites. A single spore was sown in each individual well containing FM and 0.7% (w/v) agar to produce hermaphroditic gametophytes. Hermaphrodites were imaged at 2, 3, and 5 DAG, respectively, and their phenotypes were quantitatively characterized based on high-resolution confocal images.

(legend continued on next page)





observed labeled dividing cells (green) in WT hermaphrodites, primarily located at one lateral side-the meristem initiation site (Figures 4J, 4K, and 4N). In contrast, CrHAM KD hermaphrodites exhibited fewer labeled cells, which sporadically appeared on both sides of the hermaphrodite (Figures 4L-4N). These findings indicate that cell division activity is significantly reduced or disturbed in CrHAM KD hermaphrodites during meristem initiation. We also performed confocal time-lapse imaging to examine cell division dynamics and capture each division event during hermaphrodite development (Figures 40-4Y). Starting from 2 DAG, both WT and CrHAM KD hermaphrodites were live-imaged at 6-h intervals for up to 18 h (Figures 40-4R and 4T-4W). Quantitative analysis revealed that CrHAM KD hermaphrodites had fewer cells involved in cell division and reduced total division events compared with WT hermaphrodites over the 18-h period (Figures 4S, 4X, and 4Y). Taken together, our results demonstrate that CrHAM is required for maintaining division activity during hermaphrodite development, particularly after meristem initiation, ultimately influencing prothallus size.

Transcriptomic profiling of hermaphrodites and males from WT and CrHAM KD

To comprehensively determine the downstream signaling of CrHAM in controlling gametophyte development, we performed high-throughput RNA sequencing (RNA-seq) on developing hermaphrodites and males from the same WT or *CrHAM* KD population at 5 DAG (Figure 5). Initially, we assessed all the samples included in the RNA-seq experiment. The four biological replicates for each genotype and sex type (including WT hermaphrodites, WT males, *CrHAM* KD hermaphrodites, and *CrHAM* KD males) exhibited consistent expression profiles with high correlation coefficients (Figures 5A, S4A, and S4B). Additionally, each genotype and sex type displayed distinct patterns of overall gene expression in the principal component analysis (PCA) plot (Figure 5A).

Subsequently, we identified differentially expressed genes (DEGs) in CrHAM KD (|fold change| > 2; adjusted p < 0.05) (Data S3). Specifically, there were 651 upregulated and 843 downregulated genes in CrHAM KD hermaphrodites compared with WT hermaphrodites (Figure 5B), and 493 upregulated and 614 downregulated genes in CrHAM KD males compared with WT males (Figure 5C). Additionally, we generated Venn diagrams

to illustrate both unique and overlap DEGs in *CrHAM* KD hermaphrodites and *CrHAM* KD males (Figures 5D and 5E). For example, 395 DEGs were specifically upregulated and 579 DEGs were specifically downregulated in *CrHAM* KD hermaphrodites (Figures 5D and 5E), suggesting potential hermaphrodite-specific pathways governed by CrHAM. We also analyzed the relationship between DEGs in *CrHAM* KD hermaphrodites and in sex types (Figures S4C and S4D). Venn diagrams revealed that among all the DEGs, more upregulated genes in *CrHAM* KD hermaphrodites were male-enriched (207) rather than hermaphrodite-enriched (123). In contrast, more downregulated genes in *CrHAM* KD hermaphrodites were hermaphrodite-enriched (285) rather than male-enriched (182). These transcriptomic changes were in line with our observations that *CrHAM* KD resulted in reduced female traits and increased male traits.

Gene Ontology (GO) analysis of the DEGs in *CrHAM* KD hermaphrodites (Figures 5F and 5G) and *CrHAM* KD males (Figures S4E and S4F) provided insights into the functional categories regulated by CrHAM. Notably, several GO terms in the "cellular component" (CC) and "biological process" (BP) categories (Figure 5G; Data S4), including "pectinesterase activity," "external encapsulating structure," "cell wall," and "cell wall modification," were significantly enriched in DEGs in *CrHAM* KD hermaphrodites (Figure 5G; Data S4). These enriched terms corresponded to cell wall dynamics and prothallus expansion in Ceratopteris hermaphrodites. In the category of "molecular function" (MF), the term related to "DNA binding transcription factor activity" was also significantly enriched (Figure 5G; Data S4), suggesting CrHAM mediates downstream transcriptional cascades during hermaphrodite development.

We further examined a few individuals from the list of DEGs in CrHAM KD hermaphrodites at 5 DAG (Figure 5B; Data S3). We found that one CLAVATA1 (CLV1) homolog (Ceric.11G028700, named CrCLV1a) that encodes a putative receptor for CLV3/CLE peptides and a YUCCA (YUC) homolog (Ceric.01G116200, named CrYUC1) that involves auxin biosynthesis were downregulated in CrHAM KD hermaphrodites (Figures 5H–5K; Data S2 and S3). These results were consistent with previous characterizations in the liverwort Marchantia, a different seed-free model that also forms notch meristems during the haploid gametophyte stage. The regulation of meristem development in Marchantia thalli involves both the CLV/CLE peptide signaling and phytohormone

(B-G) Confocal images of gametophytes at 2 DAG (B and E), 3 DAG (C and F), and 5 DAG (D and G). Gray: PI counterstain. Yellow arrows, meristems; yellow arrowheads, archegonia; blue arrowheads, antheridia.

(H and I) Prothallus area (H) and total cell number (I) per prothallus at different DAG. Each archegonium or antheridium was counted as one cell. Red dots represent individual WT gametophytes (n = 5, 2 DAG; n = 6, 5 DAG), blue triangles represent individual gametophytes of the *CrHAM* KD line 37 (n = 6, 2 DAG; n = 6, 5 DAG), and blue squares represent individual gametophytes of the *CrHAM* KD line 111 (n = 5, 2 DAG; n = 6, 5 DAG).

(J-M) Confocal images of the EdU-labeled gametophytes at 2 DAG. Green: EdU. Yellow arrows: meristems.

(K and M) Merged EdU (green) and differential interference contrast (DIC) (showing the cell outline).

(N) Quantification of the EdU-labeled nuclei/cells from WT and CrHAM KD gametophytes. Samples include the WT control (n = 5 biological replicates), CrHAM KD line 37 (n = 5 biological replicates), and CrHAM KD line 111 (n = 4 biological replicates).

(O–X) Time-lapse live imaging of a WT gametophyte (O–S) and a *CrHAM* KD gametophyte (T–X). Hermaphroditic gametophytes at 2 DAG were imaged on FM plates through laser confocal microscopy as the first time point (0 h). The gametophytes were live-imaged every 6 h from 0 to 18 h. Computational segmentation and quantification (S and X) show the total division events of each cell lineage projected to the segmented cells at 0 h (O and T). Colors indicate the total number of cell division events for each cell lineage during 0–18 h, with the scale from white (0) to red (4).

(Y) Quantification of cell division events during meristem establishment in Ceratopteris hermaphrodites within the 0-18 h frame. Samples include the WT control and two *CrHAM* KD lines (37 and 111), n = 6 biological replicates for each genotype.

(H, I, N, and Y) Horizontal lines represent means, and error bars indicate SEMs. *p < 0.05; **p < 0.01, ***p < 0.001 (Student's two-tailed t test). Scale bars, 100 μ m (B–G, J–M, O–R, and T–W).



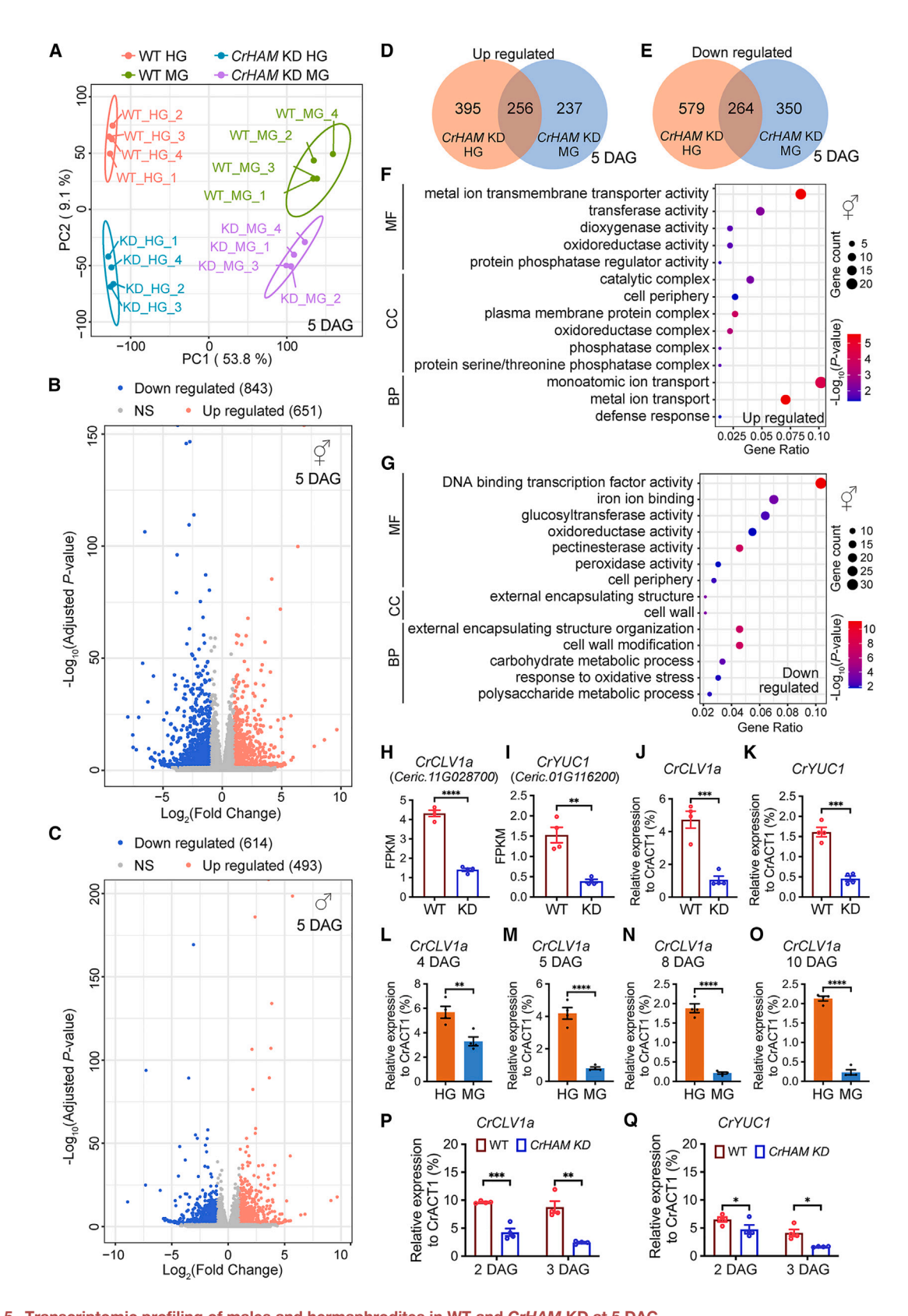


Figure 5. Transcriptomic profiling of males and hermaphrodites in WT and CrHAM KD at 5 DAG

(A) Principal component analysis (PCA) plot of biological replicates for WT and CrHAM KD (line 37) at 5 DAG. Red dots, WT hermaphroditic gametophytes (HGs); green dots, WT male gametophytes (MGs); blue dots, CrHAM KD HG; purple dots, CrHAM KD MG.





auxin-mediated signaling pathways, ^{51,52} and both *MpCLV1* and *MpYUC2* are expressed and necessary for the proliferation of undifferentiated cells in the meristem notch. ^{51,52}

We then examined the dynamic expression patterns of CrCLV1a and CrYUC1 in the two sex types at various developmental stages. Specifically, we separately collected WT hermaphrodites and males at 4, 5, 8, and 10 DAG and quantified their transcript levels using reverse-transcription qPCR (RTqPCR) analysis (Figures 5L-5O and S4G-S4J). CLV1a exhibited a higher expression level in WT hermaphrodites than males at 4 DAG (Figure 5L), and this difference became more dramatic as gametophytes developed (Figures 5M-5O), correlating with the process from meristem initiation to full establishment in hermaphrodites (from 4 to 10 DAG). CrYUC1 exhibited consistent patterns during gametophyte development, always showing higher expression in WT hermaphrodites than in WT males (Figures S4G-S4J). The expression levels of CrCLV1a and CrYUC1 were also determined in the WT and CrHAM KD gametophyte population at early developmental stages (Figures 5P and 5Q). Both genes exhibited reduced expression levels in CrHAM KD compared with the WT as early as 2 and 3 DAG, suggesting that downregulation of these two genes is an early event and likely a direct effect of the CrHAM loss of function.

CrHAM integrates multiple signaling pathways in maintaining meristem indeterminacy in hermaphrodites

To determine transcriptomic changes in *CrHAM* KD hermaphrodites at a late developmental stage in the absence of exogenous antheridiogen, we collected individually cultured WT and *CrHAM* KD hermaphrodites at 8 DAG. We performed RNA-seq and evaluated the transcriptional alterations (Figures 6A–6D and S5A–S5G). Four biological replicates for either WT or *CrHAM* KD hermaphrodites exhibited consistent expression profiles with high correlation coefficients (Figures S5A–S5C). Meanwhile, the two distinct sample types (WT vs. *CrHAM* KD) showed clearly distinguishable patterns (Figures S5A and S5B). Subsequently, we identified DEGs, with 567 upregulated and 599 downregulated genes in *CrHAM* KD hermaphrodites (Figure 6A; Data S5). Next, we generated a heatmap comparing the expression levels of DEGs identified in *CrHAM* KD hermaphrodites at 5 or 8 DAG

(Figure 6B; Data S4). The dynamic patterns of these genes revealed the developmental trajectory of hermaphrodite development when CrHAM activity was reduced (Figure 6B). We then performed the GO enrichment analysis of DEGs in *CrHAM* KD at 8 DAG (Figures 6C and 6D; Data S4). Our results demonstrated that the GO terms, including pectinesterase activity, external encapsulating structure, cell wall, cell wall modification, and DNA binding transcription factor activity, which were enriched in 5-DAG *CrHAM* KD hermaphrodites (Figure 5G; Data S4), were also significantly enriched in the 8-DAG *CrHAM* KD hermaphrodites (Figure 6D; Data S4). These findings suggested that the regulation of cell wall dynamics and transcriptional signaling cascades continued to be associated with the reduced meristem size and disturbed hermaphrodite development in *CrHAM* KD at 8 DAG.

Next, we looked at DEGs at 8 DAG. In line with the increased number of antheridia in CrHAM KD hermaphrodites, CrGAMYB1 (Ceric.02G004600) and a group of genes annotated with functions involving spermatogenesis (e.g., Ceric.29G029600, Ceric. 13G045300, and Ceric.22G060000) were upregulated in CrHAM KD hermaphrodites (Data S5), suggesting that the CrHAM loss of function also increases the sensitivity of hermaphrodites to endogenous A_{CE}. The upregulation of genes conserved in male programming in CrHAM KD hermaphrodites supports our working hypothesis that CrHAM inhibits cell differentiation, especially antheridium differentiation. In contrast, among the list of downregulated genes in CrHAM KD at 8 DAG, the significant reduction of the CrHAM level in CrHAM KD hermaphrodites revealed by RNA-seq (Figure S5D; Data S5) agreed with the gPCR results (Figure S2B). We also identified CLV1a and CrYUC1 in this list (Data S5; Figures S5E and S5F), consistent with the RNA-seq data and qPCR results at earlier developmental stages (Figures 5H-5Q and S4G-S4J). In addition to the components in hormone signaling, a group of genes encoding expansins - proteins responsible for cell wall loosening⁵³—were also downregulated in CrHAM KD hermaphrodites (Data S5: Figure S5G). This finding aligned with our results showing that CrHAM KD hermaphrodites developed less-expanded prothalli than the WT control (Figures 4B-4G and 4H). Furthermore, we quantified the expression dynamics of CrEXP1 (Ceric.05G087800), one of these

(B and C) Volcano plots illustrating upregulated genes (red dots) and downregulated genes (blue dots) in *CrHAM* KD HG compared with WT HG (B) and in *CrHAM* KD MG compared with WT MG (C). Gray dots indicate genes that are not significantly differentially expressed. The DEGs were defined based on the |fold change| >2 with an adjusted p < 0.05.

(D) Venn diagram showing the overlap between upregulated genes in CrHAM KD HG (orange, compared with WT HG) and upregulated genes in CrHAM KD MG (blue, compared with WT MG).

(E) Venn diagram showing the overlap between downregulated genes in CrHAM KD HG (orange, compared with WT HG) and downregulated genes in CrHAM KD MG (blue, compared with WT MG).

(F and G) GO enrichment analysis of upregulated (F) and downregulated (G) genes in *CrHAM* KD HG compared with WT HG. The y axis represents enriched GO terms (CC, cellular component; MF, molecular function; BP, biological process). The x axis represents the ratios of DEGs annotated to each GO term relative to the total annotated DEGs. Adjusted *p* values are color-coded from blue (less significant enrichment) to red (more significant enrichment). Solid circle sizes represent the number of DEGs annotated to each GO term.

(H and I) FPKM (fragments per kilobase per million mapped reads) of CrCLV1a (H) and CrYUC1 (I) at 5 DAG were determined by RNA-seq analysis.

(J and K) Relative expressions of the same genes at 5 DAG were determined by qPCR analysis and normalized to CrACT1. Each genotype (WT HG and CrHAM KD line 37 HG) had four biological replicates (H–K).

(L–O) Relative expressions of *CrCLV1a* at different sex types and various developmental stages were determined by qPCR analysis and normalized to *CrACT1*. Samples include WT HG and WT MG at 4 (L), 5 (M), 8 (N), and 10 (O) DAG. n = 4 biological replicates.

(P and Q) Relative expressions of CrCLV1a (P) and CrYUC1 (Q) were determined at 2 and 3 DAG by qPCR analysis and normalized to CrACT1. Samples include gametophytes of the WT and CrHAM KD (line 37). n = 4 biological replicates. Bars: means \pm SEMs. *p < 0.05; **p < 0.01; ****p < 0.001; *****p < 0.0001 (Student's two-tailed t test).

See also Figure S4 and Data S2, S3, and S4.

Current Biology



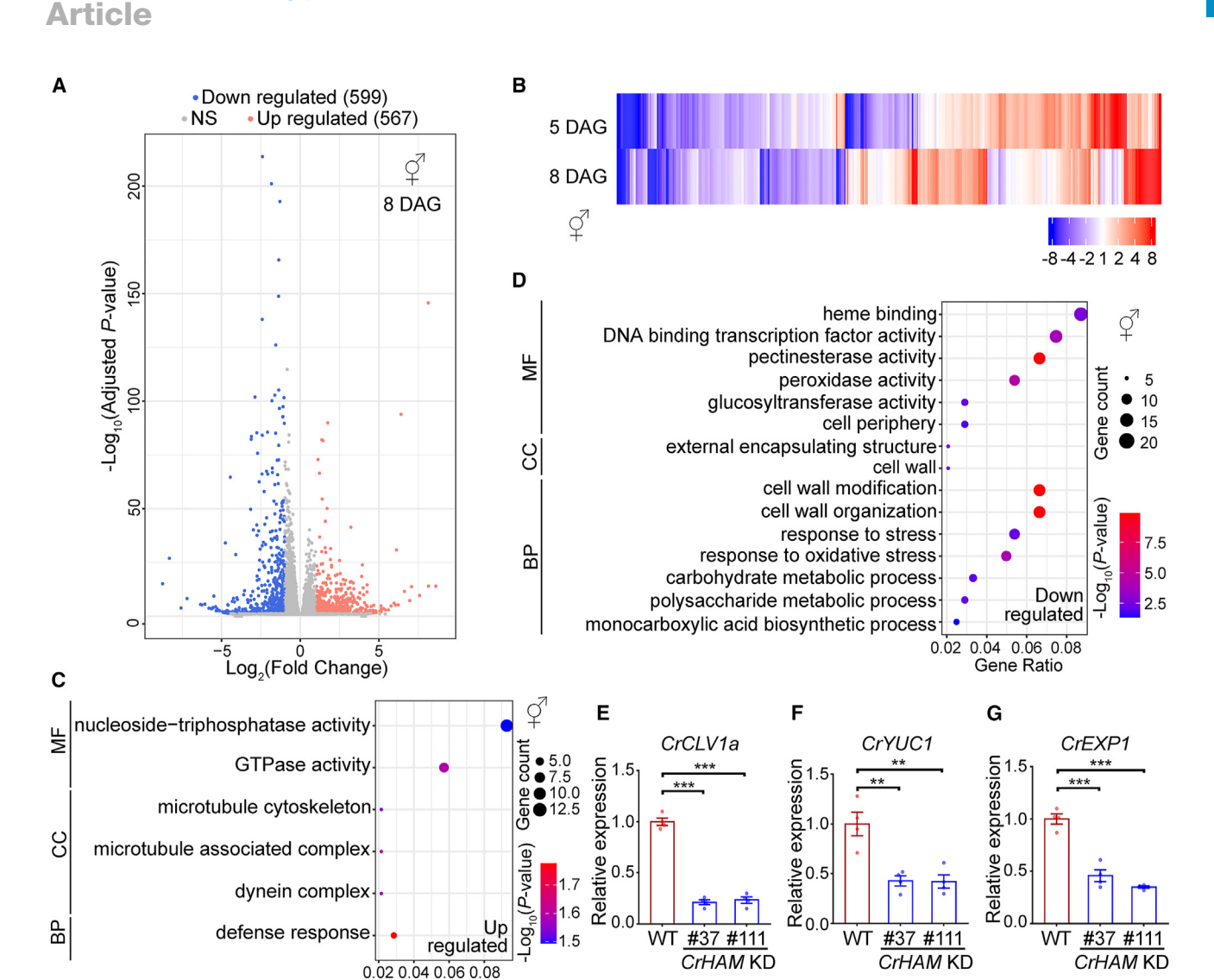


Figure 6. Gene expression profiles of hermaphrodites from WT and CrHAM KD at 8 DAG

Gene Ratio

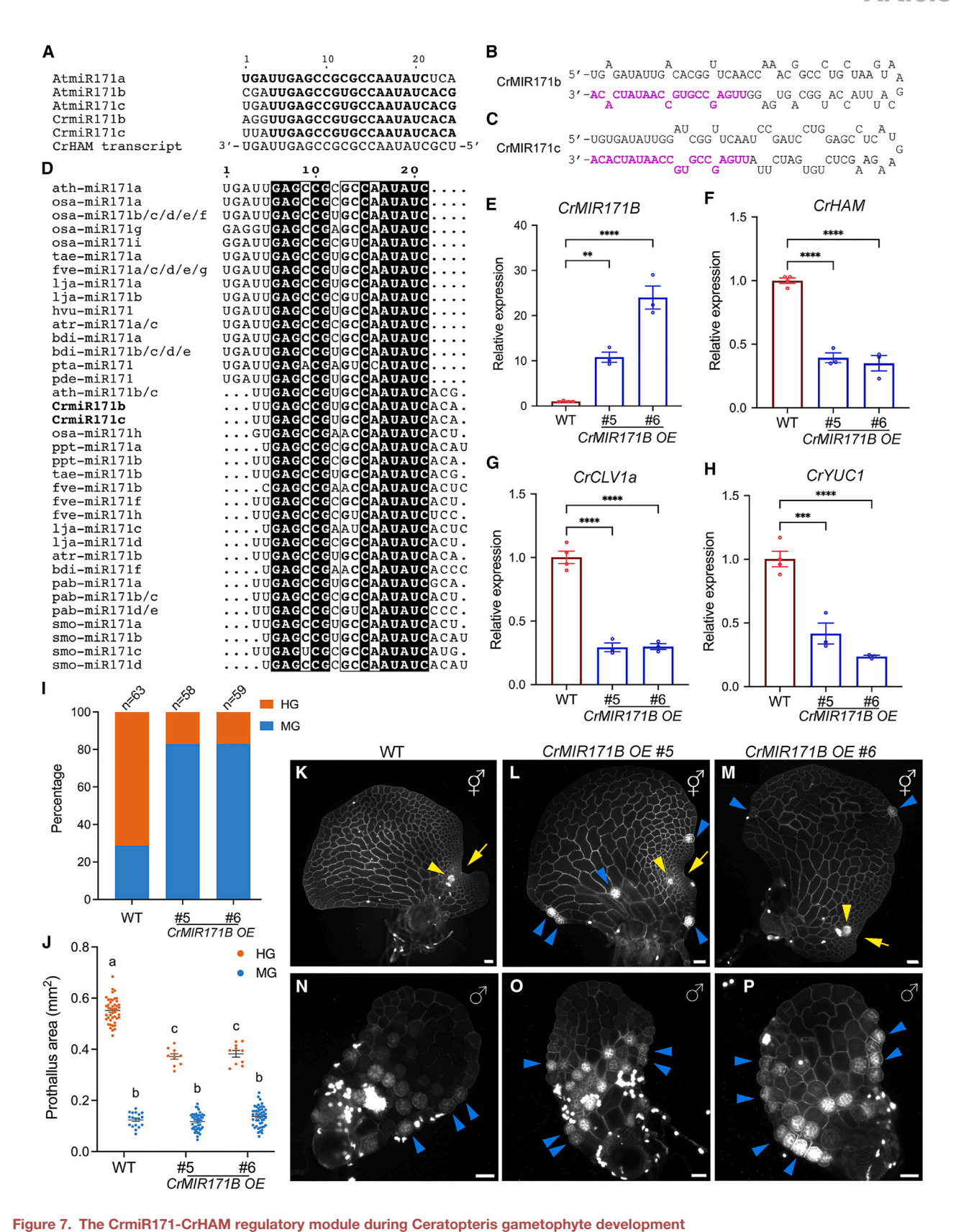
(A) Volcano plot showing upregulated genes (red dots) and downregulated genes (blue dots) in CrHAM KD HG compared with WT HG. Gray dots indicate genes that are not significantly differentially expressed. The DEGs were defined based on the |fold change| >2 with an adjusted p < 0.05. (B) Heatmap illustrating expression patterns of DEGs in CrHAM KD (line 37) HG compared with WT HG at 5 and 8 DAG. Gene expression levels are color-coded from blue (minimum, fold change ≤ -8) to red (maximum, fold change ≥ 8). Each genotype (WT and CrHAM KD line 37) had four biological replicates. (C and D) GO enrichment analysis of upregulated (C) and downregulated (D) genes in CrHAM KD HG compared with WT HG. The y axis represents enriched GO terms (CC, cellular component; MF, molecular function; BP, biological process). The x axis represents the ratios of DEGs annotated to each GO term relative to the total annotated DEGs. Adjusted p values are color-coded from blue (less significant enrichment) to red (more significant enrichment). Solid circle sizes represent the number of DEGs annotated to each GO term.

(E–G) Relative expressions of *CrCLV1a* (E), *CrYUC1* (F), and *CrEXP1* (G) were determined by qPCR analysis and normalized to *CrACT1*. Gene expression levels in *CrHAM* KD hermaphrodites were normalized to that in WT. Each genotype (WT HG, *CrHAM* KD line 37 HG, and *CrHAM* KD line 111 HG) had four biological replicates. Bars: means ± SEMs. **p < 0.01; ***p < 0.001 (Student's two-tailed t test). See also Figure S5 and Data S2, S4, and S5.

genes encoding an expansin (Data S2), in WT hermaphrodites and males at different DAG (Figures S5H–S5K). Our data consistently demonstrated that this gene was closely associated with hermaphrodites instead of males. These results were in line with the greatly expanded prothallus in WT hermaphrodites compared with males and suggested that CrEXP1 served as a hermaphrodite-specific marker at late developmental stages (Figures S5J and S5K). To independently validate the identified

DEGs, we collected an additional set of 8-DAG hermaphrodite samples and quantified relative expression levels of *CrCLV1a*, *CrYUC1*, and *CrEXP1* in the WT and *CrHAM* KD using qPCR analysis (Figures 6E–6G). All the three genes exhibited the differential expression consistent with the RNA-seq dataset (Figures 6E–6G). Taken together, these results (Figures 5, 6, S4, and S5) collectively suggest that CrHAM integrates multiple evolutionarily conserved regulatory pathways, including CLV/CLE peptide





(A) Alignment of AtmiR171 (Arabidopsis miR171), CrmiR171 (Ceratopteris miR171), and the *CrHAM* transcript. The *CrHAM* sequence is aligned in the reversed direction.



signaling, auxin signaling, and cell wall modification, to promote cell proliferation and prothallus expansion in Ceratopteris hermaphrodites.

The miR171-HAM regulatory module in Ceratopteris gametophytes

Given the crucial role of CrHAM in gametophyte development and sex differentiation, our next question was how this key meristem regulator was controlled in Ceratopteris. Previous studies in seed plants, along with our own data (Figure 1),28 suggested miR171 as a potential and specific regulator of CrHAM. Because miR171 in Ceratopteris remained to be identified, we searched for potential miR171 homologs in the Ceratopteris genome using Arabidopsis miR171 sequences as queries. Among several identified candidates, we focused on two Ceratotperis miR171 genes (named CrMIR171B and CrMIR171C) in this work (Data S6), which contained the mature microRNA sequences (CrmiR171b and CrmiR171c) nearly identical to those of Arabidopsis miR171b (AtmiR171b) and AtmiR171c (Figure 7A). Importantly, these sequences consistently aligned with the miR171-binding site²⁸ in the CrHAM transcript (Figure 7A). We also identified the predicted stem-loop structures of microRNA precursors in both CrmiR171b (Figure 7B) and CrmiR171c (Figure 7C), which also resembled those of AtmiR171b and AtmiR171c (Data S6). Additionally, we performed sequence alignment and comparison among CrmiR171b/c and miR171 previously identified in 13 species from different land plant lineages (Figure 7D; Data S6). The results demonstrated an overall high conservation of miR171 across species, with minor variations (Figure 7D).

To explore functional significance of the proposed miR171-CrHAM regulatory module in Ceratopteris gametophytes, we generated *CrMIR171B* overexpression (*CrMIR171B* OE) transgenic Ceratopteris plants by stably transforming a *35S::CrMIR171B* construct. We obtained more than ten independent transgenic lines, and, among them, two independent lines (lines 5 and 6) exhibited a significant increase in *CrMIR171B* expression. We then obtained self-fertilized sporophytes for each line and performed gene expression analysis in their gametophytes in the following generation. Compared with the WT, the hermaphrodites of the two *CrMIR171B* OE lines showed dramatically elevated *CrMIR171B* expression (Figure 7E) and a significant

reduction in the CrHAM expression (Figure 7F). Interestingly, we also found that the activation of CrMIR171B led to the repression of CrCLV1a and CrEXP1 (Figures 7G and 7H), similar to that in CrHAM KD hermaphrodites (Figures 5H-5K). We then quantified the developmental defects of these transgenic lines, along with the WT control. When grown on FM at a similar density and cultured under identical conditions, CrMIR171B OE exhibited a high male-to-hermaphrodite ratio compared with the WT, with more than 80% males in the CrMIR171B OE gametophyte population in contrast to \sim 30% males in the WT population (Figure 7I). Additionally, we stained and imaged gametophytes at 5 DAG using confocal microscopy to quantify the prothallus size and characterize gametophyte morphology (Figures 7J-7P). Although the size and morphology of CrMIR171B OE males were comparable to those of the WT (Figures 7J and 7N-7P), CrMIR171B OE hermaphrodites exhibited a small prothallus size (Figures 7J-7M), a shallow meristem notch (yellow arrows in Figures 7K-7M), a reduced meristem region (yellow arrows in Figures 7K-7M), and increased antheridium formation (blue arrowheads in Figures 7L and 7M) (Figures 7J-7M), all of which closely resembled the defects observed in CrHAM KD hermaphrodites (Figures 2 and 3). Collectively, all these data reveal that CrmiR171b negatively regulates CrHAM-mediated gametophyte development and sex determination in Ceratopteris, suggesting a conserved and functional miR171-HAM regulatory module during the gametophyte phase of Ceratopteris.

DISCUSSION

A molecular player linking meristem identity and sex determination

Green plants have evolved distinct critical pathways to control sex ratios, ^{54–56} aiming to increase genetic diversity and ensure efficient reproduction. Homosporous ferns, such as Ceratopteris, rely on pheromonal communication among individuals within the same colony to determine sex type. ¹¹ This study revealed a previously unknown mechanism underlying sex determination in Ceratopteris. It prevents hermaphrodites from transforming to ameristic males in response to antheridiogen. CrHAM plays a crucial role in this process through controlling the balance between cell division and differentiation in meristems. After the

(B and C) Secondary stem-loop structures of CrMIR171b (B) and CrMIR171c (C).

(D) Alignment of mature miR171 species from 14 land plants: Arabidopsis thaliana (ath), Amborella trichopoda (atr), Brachypodium distachyon (bdi), Ceratopteris richardii (Cr), Fragaria vesca (fve), Hordeum vulgare (hvu), Lotus japonicus (lja), Oryza sativa (osa), Picea abies (pab), Pinus densata (pde), Physcomitrella patens (ppt), Pinus taeda (pta), Selaginella moellendorffii (smo), and Triticum aestivum (tae). Nucleotides highlighted in black background indicate perfect matching, and nucleotides highlighted in frame show high conservation with an alignment score above 0.7.

(E–H) Relative expression of CrMIR171B (E), CrHAM (F), CrCLV1a (G), and CrYUC1 (H) determined by qPCR analysis, normalized to the expression levels of CrACT1. Samples include hermaphrodites of the WT control and two independent CrMIR171B overexpression (OE) transgenic lines (5 and 6). Gene expression levels in CrMIR171B OE were normalized to that in WT. n = 4 biological replicates. Bars: means \pm SEMs. **p < 0.001; ****p < 0.0001; ****p < 0.0001 (Student's two-tailed t test).

(I) Percentages of hermaphroditic gametophytes (HGs) and male gametophytes (MGs) in the gametophyte populations of WT and CrMIR171B OE.

(J) Prothallus size of gametophytes at 5 DAG in the WT and CrMIR171B OE gametophyte populations. Dots represent individual gametophytes, horizontal lines show means, and error bars represent SEMs. Differences between each of the two groups were determined by one-way ANOVA followed by Tukey's post hoc test. Values not sharing a common letter indicate significant differences (p < 0.05). (I and J) n = 63 (WT), 58 (CrMIR171B OE line 5), and 59 (CrMIR171B OE line 6), including all gametophytes from five different randomly selected 1-cm² areas for each genotype.

(K–P) Confocal images of gametophytes at 5 DAG from WT (K and N) and *CrMIR171B* OE (L, M, O, and P) populations. Gametophytes were identified as hermaphrodites with meristems (K–M) or ameristic males (N–P). Gray: PI counterstain. Yellow arrows, meristems in HG; yellow arrowheads, archegonia in HG; blue arrowheads, several antheridia in HG and MG. Scale bars, 50 μm. See also Data S6.





hermaphrodite establishes a multicellular meristem, the CrHAM protein accumulates specifically within the meristem. It promotes cell division and proliferation, inhibits male program expression, and prevents undifferentiated meristem cells from becoming sperm-producing antheridia. Thus, CrHAM serves as a link between meristem activity and sex-type expression in ferns.

Conserved regulations of HAM by miR171 in ferns and seed plants

Comparing various CrHAM fluorescent reporters indicates a conserved role of the miR171-HAM regulatory module across species and different life cycle stages, including SAMs in angiosperm sporophytes and multicellular meristems in fern gametophytes. The miR171-insensitive pCrHAM::H2B-GFP::3'CrHAM reporter showed ubiquitous expression throughout the prothalli of both hermaphrodites and males. In contrast, the miR171sensitive pCrHAM::YPET-CrHAM::3'CrHAM reporter revealed that the CrHAM protein preferentially accumulates in meristematic cells during meristem establishment and proliferation in hermaphrodites, while being excluded from differentiated cells such as antheridia (Figure 1). Therefore, it is probable that miR171 is highly accumulated or active in cells distal to meristems or within differentiated cells of Ceratopteris gametophytes, resulting in the observed CrHAM patterns (Figure 1). Additionally, the differences in CrHAM reporters mediated by miR171 in Ceratopteris gametophytes are comparable with previous findings in angiosperm sporophytes.³⁹ The miR171insensitive pAtHAM2::H2B-GFP reporter exhibits high expression in all cell layers of SAMs, whereas the miR171-sensitive pAtHAM2::YPET-AtHAM2 reporter shows high expression only in deeper layers in Arabidopsis SAMs. 39 Moreover, when the YPET-CrHAM fusion fragment was expressed under the control of the Arabidopsis HAM2 (AtHAM2) promoter and its 3' terminator, the miR171-binding site in the pAtHAM2::YPET-CrHAM reporter responded to Arabidopsis miR171, resulting in an expression pattern comparable to that of the pAtHAM2::Y-PET-AtHAM2 reporter in Arabidopsis SAMs. 28 Significantly, genetic analysis of the newly identified CrMIR171B in this study offers direct evidence supporting the functional importance of the proposed miR171-CrHAM module in Ceratopteris gametophytes. CrMIR171B OE gametophytes showed reduced expressions of CrHAM and downstream genes and exhibited developmental defects closely resembling those observed in CrHAM KD gametophytes (Figure 7). In summary, the combined evidence from previous and current studies supports the conservation of miR171-mediated downregulation of HAM between ferns and seed plants. However, the specific expression patterns and activity of Ceratopteris miR171 deserve further investigation.

Conserved roles of HAM in maintaining meristem identities

In angiosperms sporophytes, SAMs form dome-shaped structures with a conserved tunica-corpus organization, ¹ and the HAM family members play a crucial role in maintaining SAM indeterminacy and activity. ^{27,32–37} In the fern Ceratopteris, a multicellular meristem is established during the haploid gametophyte stage, and the meristem consists of a flat sheet of cells and forms a notch at its center, showing distinct morphology

compared with SAMs in angiosperm sporophytes.²² This study reveals that CrHAM is essential for maintaining meristem indeterminacy in Ceratopteris gametophytes. Within the meristems, CrHAM serves dual roles in promoting meristem development. First, CrHAM promotes cell division and proliferation to sustain meristem activity and drive notch formation, involving conserved pathways such as CLV and auxin signaling. Second, CrHAM prevents meristematic cells from differentiating into the sperm-producing antheridia, thus maintaining their undifferentiated state. Notably, our previous findings demonstrated that when YPET-CrHAM is expressed under the AtHAM2 promoter, it complements meristem defects in the Arabidopsis ham 123 triple mutant.²⁸ In addition, in the moss *Physcomitrium patens*, though comprising a single apical cell, the SAM plays equivalent roles during stem cell maintenance and organ formation.⁵⁷ When the PpGRAS12/PpHAM gene is overexpressed, multiple apical cells form ectopically at the gametophore shoot apex of Physcomitrium.⁵⁸ These results collectively highlight the ancestral and conserved role of the HAM family in maintaining meristem indeterminacy, regardless of diverse meristem structures or different developmental stages across the life cycle. It is interesting to point out that fern gametophytes maintain meristems in order to sustain hermaphrodite development and female organ formation, which are essential for reproduction. In parallel, angiosperm sporophytes develop inflorescence SAMs and floral meristems to drive floral organ development and eventually contribute to sexual reproduction. Across plant lineages separated by several hundred million years, HAM genes seem to maintain conserved roles in keeping meristems undifferentiated, which are involved in distinct strategies ensuring successful sexual reproduction.

STAR*METHODS

Detailed methods are provided in the online version of this paper and include the following:

- KEY RESOURCES TABLE
- RESOURCE AVAILABILITY
 - Lead contact
 - Materials availability
 - Data and code availability
- EXPERIMENTAL MODEL AND STUDY PARTICIPANT DETAILS
 - Ceratopteris richardii
- METHOD DETAILS
 - o Plasmid construction and plant transformation
 - o Imaging fluorescent reporters in Ceratopteris gametophytes
 - O Quantification of dynamic patterns of YPET-CrHAM
 - Reverse transcription-quantitative polymerase chain reaction (RTqPCR) analysis
 - Imaging and phenotypic characterization of CrHAM KD lines
 - o Imaging and phenotypic characterization of CrMIR171B OE lines
 - EdU staining and confocal microscopy
 - Sequence retrieval and phylogenetic analyses
 - o miR171 sequence analysis
 - RNA sequencing and analysis
- QUANTIFICATION AND STATISTICAL ANALYSIS

SUPPLEMENTAL INFORMATION

Supplemental information can be found online at https://doi.org/10.1016/j.cub.2024.06.064.

⊘ CellPress

ACKNOWLEDGMENTS

The authors thank Purdue Bindley Bioscience Facility for the access to the ZEISS LSM880 confocal microscope. This work was supported by NSF IOS 1931114 grant (to Y.Z.), NIH grant R35GM138016 (to X.L.), and the Hatch fund 7004898 from USDA-NIFA (to X.L.).

AUTHOR CONTRIBUTIONS

Y.G. and Y.Z. conceived the research direction; Y.Z. supervised the research progress; Y.G., C.X., X.Y., and D.N.L. performed experiments; Y.G., C.X., X.L., and Y.Z. discussed and interpreted results; C.X. and Y.G. performed RNA-seq data analysis; A.Y., Y.Z., and Y.G. performed image analysis; Y.G., C.X., and Y.Z. wrote the manuscript; and X.L., X.Y., and A.Y. revised the manuscript. All the authors read and approved the manuscript.

DECLARATION OF INTERESTS

The authors declare no competing interests.

Received: September 15, 2023 Revised: May 16, 2024 Accepted: June 25, 2024 Published: July 25, 2024

REFERENCES

- Meyerowitz, E.M. (1997). Genetic control of cell division patterns in developing plants. Cell 88, 299–308. https://doi.org/10.1016/s0092-8674(00) 81868-1.
- Heidstra, R., and Sabatini, S. (2014). Plant and animal stem cells: similar yet different. Nat. Rev. Mol. Cell Biol. 15, 301–312. https://doi.org/10. 1038/nrm3790.
- Steeves, T.A., and Sussex, I.M. (1989). Patterns in Plant Development, Second Edition (Cambridge University Press).
- 4. Yadegari, R., and Drews, G.N. (2004). Female gametophyte development. Plant Cell 16, S133–S141. https://doi.org/10.1105/tpc.018192.
- McCormick, S. (2004). Control of male gametophyte development. Plant Cell 16, S142–S153. https://doi.org/10.1105/tpc.016659.
- Banks, J.A. (1999). Gametophyte development in ferns. Annu. Rev. Plant Physiol. Plant Mol. Biol. 50, 163–186. https://doi.org/10.1146/annurev.arplant.50.1.163.
- Imaichi, R. (2013). Review a new classification of the gametophyte development of homosporous ferns, focusing on meristem behaviour. Fern Gaz. 19, 141–156.
- Nayar, B.K., and Kaur, S. (1971). Gametophytes of homosporous ferns. Bot. Rev. 37, 295–396. https://doi.org/10.1007/BF02859157.
- Geng, Y., Cai, C., McAdam, S.A.M., Banks, J.A., Wisecaver, J.H., and Zhou, Y. (2021). A de novo transcriptome assembly of Ceratopteris richardii provides insights into the evolutionary dynamics of complex gene families in land plants. Genome Biol. Evol. 13, evab042. https://doi.org/10. 1093/gbe/evab042.
- Kinosian, S.P., and Wolf, P.G. (2022). The biology of *C. richardii* as a tool to understand plant evolution. eLife 11, e75019. https://doi.org/10.7554/ eLife.75019.
- Atallah, N.M., and Banks, J.A. (2015). Reproduction and the pheromonal regulation of sex type in fern gametophytes. Front. Plant Sci. 6, 100. https://doi.org/10.3389/fpls.2015.00100.
- Conway, S.J., and Di Stilio, V.S. (2020). An ontogenetic framework for functional studies in the model fern Ceratopteris richardii. Dev. Biol. 457, 20–29. https://doi.org/10.1016/j.ydbio.2019.08.017.
- Bui, L.T., Pandzic, D., Youngstrom, C.E., Wallace, S., Irish, E.E., Szövényi, P., and Cheng, C.-L. (2017). A fern AINTEGUMENTA gene mirrors BABY BOOM in promoting apogamy in Ceratopteris richardii. Plant J. 90, 122–132. https://doi.org/10.1111/tpj.13479.

- Bui, L.T., Cordle, A.R., Irish, E.E., and Cheng, C.-L. (2015). Transient and stable transformation of *Ceratopteris richardii* gametophytes. BMC Res. Notes 8, 214. https://doi.org/10.1186/s13104-015-1193-x.
- Marchant, D.B., Chen, G., Cai, S., Chen, F., Schafran, P., Jenkins, J., Shu, S., Plott, C., Webber, J., Lovell, J.T., et al. (2022). Dynamic genome evolution in a model fern. Nat. Plants 8, 1038–1051. https://doi.org/10.1038/s41477-022-01226-7
- Plackett, A.R.G., Conway, S.J., Hewett Hazelton, K.D., Rabbinowitsch, E.H., Langdale, J.A., and Di Stilio, V.S. (2018). LEAFY maintains apical stem cell activity during shoot development in the fern Ceratopteris richardii. eLife 7, e39625.
- McAdam, S.A.M., Brodribb, T.J., Banks, J.A., Hedrich, R., Atallah, N.M., Cai, C., Geringer, M.A., Lind, C., Nichols, D.S., Stachowski, K., et al. (2016). Abscisic acid controlled sex before transpiration in vascular plants. Proc. Natl. Acad. Sci. USA 113, 12862–12867. https://doi.org/10.1073/pnas.1606614113.
- Salmi, M.L., Bushart, T.J., Stout, S.C., and Roux, S.J. (2005). Profile and analysis of gene expression changes during early development in germinating spores of *Ceratopteris richardii*. Plant Physiol. 138, 1734–1745. https://doi.org/10.1104/pp.105.062851.
- Chatterjee, A., and Roux, S.J. (2000). Ceratopteris richardii: a productive model for revealing secrets of signaling and development. J. Plant Growth Regul. 19, 284–289. https://doi.org/10.1007/s003440000032.
- Banks, J.A., Hickok, L., and Webb, M.A. (1993). The programming of sexual phenotype in the homosporous fern *Ceratopteris richardii*. Int. J. Plant Sci. 154, 522–534. https://doi.org/10.1086/297135.
- Hickok, L.G., Warne, T.R., and Slocum, M.K. (1987). Ceratopteris richardii: applications for experimental plant biology. Am. J. Bot. 74, 1304–1316. https://doi.org/10.1002/j.1537-2197.1987.tb08743.x.
- Geng, Y., Yan, A., and Zhou, Y. (2022). Positional cues and cell division dynamics drive meristem development and archegonium formation in Ceratopteris gametophytes. Commun. Biol. 5, 650. https://doi.org/10.1038/s42003-022-03627-y.
- Banks, J.A. (1997). The TRANSFORMER genes of the fern Ceratopteris simultaneously promote meristem and archegonia development and repress antheridia development in the developing gametophyte. Genetics 147, 1885–1897. https://doi.org/10.1093/genetics/147.4.1885.
- Banks, J.A. (1994). Sex-determining genes in the homosporous fern Ceratopteris. Development 120, 1949–1958. https://doi.org/10.1242/ dev.120.7.1949.
- Tanurdzic, M., and Banks, J.A. (2004). Sex-determining mechanisms in land plants. Plant Cell 16, S61–S71. https://doi.org/10.1105/tpc.016667.
- Strain, E., Hass, B., and Banks, J.A. (2001). Characterization of mutations that feminize gametophytes of the fern Ceratopteris. Genetics 159, 1271– 1281. https://doi.org/10.1093/genetics/159.3.1271.
- Schulze, S., Schäfer, B.N., Parizotto, E.A., Voinnet, O., and Theres, K. (2010). LOST MERISTEMS genes regulate cell differentiation of central zone descendants in Arabidopsis shoot meristems. Plant J. 64, 668–678. https://doi.org/10.1111/j.1365-313X.2010.04359.x.
- Geng, Y., Guo, L., Han, H., Liu, X., Banks, J.A., Wisecaver, J.H., and Zhou, Y. (2021). Conservation and diversification of *HAIRY MERISTEM* gene family in land plants. Plant J. 106, 366–378. https://doi.org/10.1111/tpj. 15169.
- Engstrom, E.M., Andersen, C.M., Gumulak-Smith, J., Hu, J., Orlova, E., Sozzani, R., and Bowman, J.L. (2011). Arabidopsis homologs of the Petunia *HAIRY MERISTEM* gene are required for maintenance of shoot and root indeterminacy. Plant Physiol. 155, 735–750. https://doi.org/10. 1104/pp.110.168757.
- Han, H., Liu, X., and Zhou, Y. (2020). Transcriptional circuits in control of shoot stem cell homeostasis. Curr. Opin. Plant Biol. 53, 50–56. https:// doi.org/10.1016/j.pbi.2019.10.004.
- Geng, Y., and Zhou, Y. (2021). HAM gene family and shoot meristem development. Front. Plant Sci. 12, 800332. https://doi.org/10.3389/fpls. 2021.800332.



Current Biology

- 32. Han, H., Geng, Y., Guo, L., Yan, A., Meyerowitz, E.M., Liu, X., and Zhou, Y. (2020). The overlapping and distinct roles of HAM family genes in Arabidopsis shoot meristems. Front. Plant Sci. 11, 541968. https://doi. org/10.3389/fpls.2020.541968.
- 33. Zhou, Y., Yan, A., Han, H., Li, T., Geng, Y., Liu, X., and Meyerowitz, E.M. (2018). HAIRY MERISTEM with WUSCHEL confines CLAVATA3 expression to the outer apical meristem layers. Science 361, 502-506. https:// doi.org/10.1126/science.aar8638.
- 34. Zhou, Y., Liu, X., Engstrom, E.M., Nimchuk, Z.L., Pruneda-Paz, J.L., Tarr, P.T., Yan, A., Kay, S.A., and Meyerowitz, E.M. (2015). Control of plant stem cell function by conserved interacting transcriptional regulators. Nature 517, 377-380. https://doi.org/10.1038/nature13853.
- 35. David-Schwartz, R., Borovsky, Y., Zemach, H., and Paran, I. (2013). CaHAM is autoregulated and regulates CaSTM expression and is required for shoot apical meristem organization in pepper. Plant Sci. 203, 8-16. https://doi.org/10.1016/j.plantsci.2012.12.011.
- 36. Wang, L., Mai, Y.X., Zhang, Y.C., Luo, Q., and Yang, H.Q. (2010). MicroRNA171c-targeted SCL6-II, SCL6-III, and SCL6-IV genes regulate shoot branching in Arabidopsis. Mol. Plant 3, 794-806. https://doi.org/ 10.1093/mp/ssq042.
- 37. Stuurman, J., Jäggi, F., and Kuhlemeier, C. (2002). Shoot meristem maintenance is controlled by a GRAS-gene mediated signal from differentiating cells. Genes Dev. 16, 2213-2218. https://doi.org/10.1101/gad.230702.
- 38. Han, H., and Zhou, Y. (2022). Function and regulation of microRNA171 in plant stem cell homeostasis and developmental programing. Int. J. Mol. Sci. 23, 2544. https://doi.org/10.3390/ijms23052544.
- 39. Han, H., Yan, A., Li, L., Zhu, Y., Feng, B., Liu, X., and Zhou, Y. (2020). A signal cascade originated from epidermis defines apical-basal patterning of Arabidopsis shoot apical meristems. Nat. Commun. 11, 1214. https:// doi.org/10.1038/s41467-020-14989-4.
- 40. Rhoades, M.W., Reinhart, B.J., Lim, L.P., Burge, C.B., Bartel, B., and Bartel, D.P. (2002). Prediction of plant microRNA targets. Cell 110, 513-520. https://doi.org/10.1016/s0092-8674(02)00863-2.
- 41. Llave, C., Xie, Z., Kasschau, K.D., and Carrington, J.C. (2002). Cleavage of Scarecrow-like mRNA targets directed by a class of Arabidopsis miRNA. Science 297, 2053-2056. https://doi.org/10.1126/science.1076311.
- 42. Geng, Y., and Zhou, Y. (2021). N-terminal region is required for functions of the HAM family member. Plant Signal. Behav. 16, 1940001. https://doi. org/10.1080/15592324.2021.1940001.
- 43. Miki, D., and Shimamoto, K. (2004). Simple RNAi vectors for stable and transient suppression of gene function in rice. Plant Cell Physiol. 45, 490-495. https://doi.org/10.1093/pcp/pch048.
- 44. Murray, F., Kalla, R., Jacobsen, J., and Gubler, F. (2003). A role for HvGAMYB in anther development. Plant J. 33, 481-491. https://doi.org/ 10.1046/j.1365-313x.2003.01641.x.
- 45. Kaneko, M., Inukai, Y., Ueguchi-Tanaka, M., Itoh, H., Izawa, T., Kobayashi, Y., Hattori, T., Miyao, A., Hirochika, H., Ashikari, M., and Matsuoka, M. (2004). Loss-of-function mutations of the rice GAMYB gene impair alpha-amylase expression in aleurone and flower development. Plant Cell 16, 33-44. https://doi.org/10.1105/tpc.017327.
- 46. Aya, K., Ueguchi-Tanaka, M., Kondo, M., Hamada, K., Yano, K., Nishimura, M., and Matsuoka, M. (2009). Gibberellin modulates anther development in rice via the transcriptional regulation of GAMYB. Plant Cell 21, 1453-1472. https://doi.org/10.1105/tpc.108.062935.
- 47. Tanaka, J., Yano, K., Aya, K., Hirano, K., Takehara, S., Koketsu, E., Ordonio, R.L., Park, S.-H., Nakajima, M., Ueguchi-Tanaka, M., and Matsuoka, M. (2014). Antheridiogen determines sex in ferns via a spatiotemporally split gibberellin synthesis pathway. Science 346, 469-473. https://doi.org/10.1126/science.1259923.
- 48. Yamane, H. (1998). Fern Antheridiogens. In International Review of Cytology, 184, K.W. Jeon, ed. (Academic Press), pp. 1-32.
- 49. Salic, A., and Mitchison, T.J. (2008). A chemical method for fast and sensitive detection of DNA synthesis in vivo. Proc. Natl. Acad. Sci. USA 105, 2415-2420. https://doi.org/10.1073/pnas.0712168105.

- 50. Kotogány, E., Dudits, D., Horváth, G.V., and Ayaydin, F. (2010). A rapid and robust assay for detection of S-phase cell cycle progression in plant cells and tissues by using ethynyl deoxyuridine. Plant Methods 6, 5. https://doi. org/10.1186/1746-4811-6-5.
- 51. Eklund, D.M., Ishizaki, K., Flores-Sandoval, E., Kikuchi, S., Takebayashi, Y., Tsukamoto, S., Hirakawa, Y., Nonomura, M., Kato, H., Kouno, M., et al. (2015). Auxin produced by the indole-3-pyruvic acid pathway regulates development and gemmae dormancy in the liverwort Marchantia polymorpha. Plant Cell 27, 1650-1669. https://doi.org/10.1105/tpc.15. 00065.
- 52. Hirakawa, Y., Fujimoto, T., Ishida, S., Uchida, N., Sawa, S., Kiyosue, T., Ishizaki, K., Nishihama, R., Kohchi, T., and Bowman, J.L. (2020). Induction of multichotomous branching by CLAVATA peptide in Marchantia polymorpha. Curr. Biol. 30, 3833-3840.e4. https://doi.org/ 10.1016/j.cub.2020.07.016.
- 53. Cosgrove, D.J. (2015). Plant expansins: diversity and interactions with plant cell walls. Curr. Opin. Plant Biol. 25, 162-172. https://doi.org/10. 1016/j.pbi.2015.05.014.
- 54. Coelho, S.M., and Umen, J. (2021). Switching it up: algal insights into sexual transitions. Plant Reprod. 34, 287-296. https://doi.org/10.1007/ s00497-021-00417-0.
- 55. Grant, S., Houben, A., Vyskot, B., Siroky, J., Pan, W.-H., Macas, J., and Saedler, H. (1994). Genetics of sex determination in flowering plants. Dev. Genet. 15, 214-230. https://doi.org/10.1002/dvg.1020150304.
- 56. Ainsworth, C., Parker, j., and Buchanan-Wollaston, V. (1997). 5 Sex determination in plants. In Current Topics in Developmental Biology, 38, R.A. Pedersen, and G.P. Schatten, eds. (Academic Press), pp. 167-223.
- 57. Harrison, C.J., Roeder, A.H.K., Meyerowitz, E.M., and Langdale, J.A. (2009). Local cues and asymmetric cell divisions underpin body plan transitions in the moss Physcomitrella patens. Curr. Biol. 19, 461-471. https:// doi.org/10.1016/j.cub.2009.02.050.
- 58. Beheshti, H., Strotbek, C., Arif, M.A., Klingl, A., Top, O., and Frank, W. (2021). PpGRAS12 acts as a positive regulator of meristem formation in Physcomitrium patens. Plant Mol. Biol. 107, 293-305. https://doi.org/10. 1007/s11103-021-01125-z.
- 59. Barrell, P.J., and Conner, A.J. (2006). Minimal T-DNA vectors suitable for agricultural deployment of transgenic plants. BioTechniques 41, 708-710. https://doi.org/10.2144/000112306.
- 60. Curtis, M.D., and Grossniklaus, U. (2003). A gateway cloning vector set for high-throughput functional analysis of genes in planta. Plant Physiol. 133, 462-469. https://doi.org/10.1104/pp.103.027979.
- 61. Schindelin, J., Arganda-Carreras, I., Frise, E., Kaynig, V., Longair, M., Pietzsch, T., Preibisch, S., Rueden, C., Saalfeld, S., Schmid, B., et al. (2012). Fiji: an open-source platform for biological-image analysis. Nat. Methods 9, 676-682. https://doi.org/10.1038/nmeth.2019.
- 62. Li, F.-W., Brouwer, P., Carretero-Paulet, L., Cheng, S., de Vries, J., Delaux, P.-M., Eily, A., Koppers, N., Kuo, L.-Y., Li, Z., et al. (2018). Fern genomes elucidate land plant evolution and cyanobacterial symbioses. Nat. Plants 4, 460-472. https://doi.org/10.1038/s41477-018-0188-8.
- 63. Kozomara, A., and Griffiths-Jones, S. (2014). miRBase: annotating high confidence microRNAs using deep sequencing data. Nucleic Acids Res. 42, D68-D73. https://doi.org/10.1093/nar/gkt1181.
- 64. Emms, D.M., and Kelly, S. (2019). OrthoFinder: phylogenetic orthology inference for comparative genomics. Genome Biol. 20, 238. https://doi. org/10.1186/s13059-019-1832-y.
- 65. Van Bel, M., Silvestri, F., Weitz, E.M., Kreft, L., Botzki, A., Coppens, F., and Vandepoele, K. (2022). PLAZA 5.0: extending the scope and power of comparative and functional genomics in plants. Nucleic Acids Res. 50, D1468-D1474. https://doi.org/10.1093/nar/gkab1024.
- 66. Katoh, K., Rozewicki, J., and Yamada, K.D. (2019). MAFFT online service: multiple sequence alignment, interactive sequence choice and visualization. Brief. Bioinform. 20, 1160-1166. https://doi.org/10.1093/bib/bbx108.
- 67. Nguyen, L.-T., Schmidt, H.A., von Haeseler, A., and Minh, B.Q. (2015), IQ-TREE: a fast and effective stochastic algorithm for estimating

Current Biology Article



- maximum-likelihood phylogenies. Mol. Biol. Evol. 32, 268–274. https://doi.org/10.1093/molbev/msu300.
- Letunic, I., and Bork, P. (2019). Interactive Tree Of Life (iTOL) v4: recent updates and new developments. Nucleic Acids Res. 47, W256–W259. https://doi.org/10.1093/nar/gkz239.
- Tamura, K., Stecher, G., and Kumar, S. (2021). MEGA11: Molecular Evolutionary Genetics Analysis Version 11. Mol. Biol. Evol. 38, 3022–3027.
- Markham, N.R., and Zuker, M. (2008). UNAFold: software for nucleic acid folding and hybridization. Methods Mol. Biol. 453, 3–31. https://doi.org/ 10.1007/978-1-60327-429-6 1.
- Kim, D., Paggi, J.M., Park, C., Bennett, C., and Salzberg, S.L. (2019). Graph-based genome alignment and genotyping with HISAT2 and HISAT-genotype. Nat. Biotechnol. 37, 907–915. https://doi.org/10.1038/ s41587-019-0201-4.
- Liao, Y., Smyth, G.K., and Shi, W. (2014). featureCounts: an efficient general-purpose program for assigning sequence reads to genomic features. Bioinformatics 30, 923–930. https://doi.org/10.1093/bioinformatics/btt656.
- Wickham, H. (2016). ggplot2 Elegant Graphics For Data Analysis, Second Edition (Springer Press)).
- 74. Kolde, R. (2019). Pheatmap: pretty heatmaps. R package version 1, 726.
- Love, M.I., Huber, W., and Anders, S. (2014). Moderated estimation of fold change and dispersion for RNA-seq data with DESeq2. Genome Biol. 15, 550. https://doi.org/10.1186/s13059-014-0550-8.
- Chen, H., and Boutros, P.C. (2011). VennDiagram: a package for the generation of highly-customizable Venn and Euler diagrams in R. BMC Bioinformatics 12, 35. https://doi.org/10.1186/1471-2105-12-35.
- Wu, T., Hu, E., Xu, S., Chen, M., Guo, P., Dai, Z., Feng, T., Zhou, L., Tang, W., Zhan, L., et al. (2021). clusterProfiler 4.0: A universal enrichment tool for interpreting omics data. Innovation (Camb) 2, 100141. https://doi.org/10.1016/j.xinn.2021.100141.
- Sayols, S. (2023). rrvgo: a Bioconductor package to reduce and visualize Gene Ontology terms. MicroPubl Biol. https://doi.org/10.17912/micro-pub.biology.000811.
- Plackett, A.R.G., Rabbinowitsch, E.H., and Langdale, J.A. (2015).
 Protocol: genetic transformation of the fern Ceratopteris richardii through

- microparticle bombardment. Plant Methods 11, 37. https://doi.org/10.1186/s13007-015-0080-8.
- Plackett, A.R.G., Huang, L., Sanders, H.L., and Langdale, J.A. (2014).
 High-efficiency stable transformation of the model fern species *Ceratopteris richardii* via microparticle bombardment. Plant Physiol. 165, 3–14. https://doi.org/10.1104/pp.113.231357.
- Wu, X., Yan, A., Liu, X., Zhang, S., and Zhou, Y. (2022). Quantitative liveimaging reveals the dynamics of apical cells during gametophyte development in ferns. Quant. Plant Biol. 3, e25. https://doi.org/10.1017/qpb. 2022.21.
- Wu, X., Yan, A., Yang, X., Banks, J.A., Zhang, S., and Zhou, Y. (2022). Cell growth dynamics in two types of apical meristems in fern gametophytes. Plant J. 111, 149–163. https://doi.org/10.1111/tpj.15784.
- Vincent, L., and Soille, P. (1991). Watersheds in digital spaces: an efficient algorithm based on immersion simulations. IEEE Trans. Pattern Anal. Machine Intell. 13, 583–598. https://doi.org/10.1109/34.87344.
- Jiang, C.K., and Rao, G.Y. (2020). Insights into the diversification and evolution of R2R3-MYB transcription factors in plants. Plant Physiol. 183, 637–655. https://doi.org/10.1104/pp.19.01082.
- Poulet, A., and Kriechbaumer, V. (2017). Bioinformatics analysis of phylogeny and transcription of TAA/YUC auxin biosynthetic genes. Int. J. Mol. Sci. 18, 1791. https://doi.org/10.3390/ijms18081791.
- Zhao, Y., Hu, Y., Dai, M., Huang, L., and Zhou, D.X. (2018). The YUCCA-Auxin-WOX11 module controls crown root development in rice. Front. Plant Sci. 9, 523.
- 87. Smit, M.E., McGregor, S.R., Sun, H., Gough, C., Bågman, A.-M., Soyars, C.L., Kroon, J.T.M., Gaudinier, A., Williams, C.J., Yang, X., et al. (2015). A PXY-mediated pathway for cellular communication during xylem differentiation in Arabidopsis. Plant Cell 27, 1650–1669.
- 88. Minh, B.Q., Nguyen, M.A.T., and von Haeseler, A. (2013). Ultrafast approximation for phylogenetic Bootstrap. Mol. Biol. Evol. 30, 1188–1195. https://doi.org/10.1093/molbev/mst024.
- Kalyaanamoorthy, S., Minh, B.Q., Wong, T.K.F., von Haeseler, A., and Jermiin, L.S. (2017). ModelFinder: fast model selection for accurate phylogenetic estimates. Nat. Methods 14, 587–589. https://doi.org/10.1038/nmeth.4285.





STAR***METHODS**

KEY RESOURCES TABLE

REAGENT or RESOURCE	SOURCE	IDENTIFIER
Chemicals, peptides, and recombinant proteins		
Murashige & Skoog Basal Medium with Vitamins	PhytoTechnology Laboratories	Cat#M519
Agar	Sigma-Aldrich	Cat#A1296
Bleach	Clorox	N/A
Tween 20	Sigma-Aldrich	Cat#P9416
Hygromycin B	Invitrogen	Cat#10687010
Spermidine	Sigma-Aldrich	Cat#S0266
Propidium iodide	Thermo Scientific	Cat#J66764.MC
Critical commercial assays		
Click-iT Plus EdU (5-ethynyl-2'-deoxyuridine)	Thermo Scientific	Cat#C10632
Alexa Fluor 488 Imaging Kit		
RNeasy Mini Kit	Qiagen	Cat#74106
RQ1 RNase-Free DNase	Promega	Cat#M6101
SuperScript II Reverse Transcriptase	Invitrogen	Cat#18064014
RNaseOUT Recombinant Ribonuclease Inhibitor	Invitrogen	Cat#10777019
2 × SYBR Green qPCR Master Mix	Selleck Chemicals	Cat#B21203
Gateway LR Clonase II Enzyme mix	Thermo Scientific	Cat#11791020
RNA ScreenTape Analysis	Agilent	Cat#5067-5576; Cat#5067-5577; Cat#5067-5576
Deposited data		
Raw RNA-seq data	This paper	NCBI BioProject: PRJNA1121398; SRA: SRR29324678-SRR29324701
Experimental models: Organisms/strains		
Ceratopteris richardii: Hn-n	Hickok et al. ²¹	N/A
Ceratopteris richardii: Hn-n: oCrHAM::H2B-GFP::3'CrHAM	Geng et al. ²²	N/A
Ceratopteris richardii: Hn-n: oCrHAM::YPET-CrHAM::3'CrHAM	This paper	N/A
Ceratopteris richardii: Hn-n: CrHAM KD	This paper	N/A
Ceratopteris richardii: Hn-n: CrMIR171B OE	This paper	N/A
Oligonucleotides		
Primers used in this paper, see Table S2	This paper	N/A
Recombinant DNA		
pMOA34	Barrell et al. ⁵⁹	N/A
pCR8	Invitrogen	Cat#K250020
pANDA35HK	Miki et al. ⁴³	N/A
pMDC32	Curtis et al. ⁶⁰	N/A
Plasmid: <i>pCrHAM::H2B-GFP::3'CrHAM</i>	Geng et al. ²²	N/A
Plasmid: pCrHAM::YPET-CrHAM::3'CrHAM	This paper	N/A
Plasmid: CrHAM KD	This paper	N/A
Plasmid: CrMIR171B OE	This paper	N/A
Software and algorithms		
Fiji/ImageJ	Schindelin et al. ⁶¹	https://imagej.net/ij/; RRID:SCR_003070
Ceratopteris richardii genome v2.1	Marchant et al. ¹⁵	https://phytozome-next.jgi.doe.gov/info/Crichardii_v2_1
FernBase	Li et al. ⁶²	https://fernbase.org/
miRBase	Kozomara et al. ⁶³	https://mirbase.org/

(Continued on next page)

Current Biology



Article

Continued		
REAGENT or RESOURCE	SOURCE	IDENTIFIER
OrthoFinder	Emms et al. ⁶⁴	N/A
PLAZA	Van Bel et al. ⁶⁵	https://bioinformatics.psb.ugent.be/plaza
MAFFT (version 7)	Katoh et al. ⁶⁶	https://mafft.cbrc.jp/alignment/software/
IQ-TREE (version 2.2.0)	Nguyen et al. ⁶⁷	http://www.iqtree.org/
Interactive Tree of Life (iTOL)	Letunic et al. ⁶⁸	https://itol.embl.de/
MEGA 11	Tamura et al. ⁶⁹	https://www.megasoftware.net/home
The UNAFold Web Server	Markham et al. ⁷⁰	http://www.unafold.org/
Hisat2 v2.0.5 R package	Kim et al. ⁷¹	https://github.com/DaehwanKimLab/hisat2
FeatureCounts v1.5.0-p3 R package	Liao et al. ⁷²	https://subread.sourceforge.net/
ggplot2 package	Wickham ⁷³	https://github.com/tidyverse/ggplot2
pheatmap R package	Kolde ⁷⁴	https://github.com/raivokolde/pheatmap
DESeq2 R package	Love et al. ⁷⁵	https://bioconductor.org/packages/ release/bioc/html/DESeq2.html
VennDiagram R package	Chen et al. ⁷⁶	https://cran.r-project.org/web/ packages/VennDiagram/index.html
clusterProfiler R package	Wu et al. ⁷⁷	https://bioconductor.org/packages/ release/bioc/html/clusterProfiler.html
rrvgo R package	Sayols ⁷⁸	https://bioconductor.org/packages/ release/bioc/html/rrvgo.html
MATLAB code for 2D image analysis (see Data S7)	This paper	N/A
GraphPad Prism 9	GraphPad Software	https://www.graphpad.com/
Microsoft Excel	Microsoft	N/A
Other		
100 mm Petri Dish	VWR	Cat#25384-088; Cat#89107-632
60 mm Petri Dish	DOT Scientific	Cat#PD-94055
48-well tissue culture plate	Celltreat	Cat#229148
Plastic Bags	Ziploc	N/A
Needles	BD	Cat#305155
Growth Chamber	Percival	N/A
nnova 2100 Platform Shaker	New Brunswick Scientific	Cat#14-278-108
Biolistic PDS-1000/He Particle Delivery System	Bio-Rad	Cat#1652257
Upright Confocal Laser Scanning Microscope	ZEISS	Cat#LSM880
Compact Inverted Microscope for Cell Culture	Olympus	Cat#CKX53
MIchrome 5 Pro camera	Tucsen	N/A
LightCycler 96 system	Roche	Cat#05815916001
CFX Duet Real-Time PCR System	Bio-Rad	Cat#12016265

RESOURCE AVAILABILITY

Lead contact

For additional information and requests regarding resources and reagents should be directed to and will be fulfilled by the lead contact, Yun Zhou (zhouyun@purdue.edu).

Materials availability

All plasmids and spores used in this study are available upon request.

Data and code availability

RNA-seq raw data have bene deposited at the NCBI Sequence Read Archive (SRA) and are publicly available as of the date of
publication. Accession numbers are listed in key resources table (BioProject accession number: PRJNA1121398; SRA accession numbers for individual samples: from SRR29324678 to SRR29324701). The analyzed RNA-seq results are included in the
supplemental information (Data S3, S4, and S5).





- Confocal images of all gametophytes from the WT and CrHAM KD #37 examined in each 1-cm² area are included in Data S1. All
 other microscopy data reported in this paper are available from the lead contact upon request.
- The MATLAB code used for 2D segmentation and visualization of division activity is available in this paper's supplemental information (Data S7).
- Any additional information required to reanalyze the data reported in this paper is available from the lead contact upon request.

EXPERIMENTAL MODEL AND STUDY PARTICIPANT DETAILS

Ceratopteris richardii

This study used the *Ceratopteris richardii* accession Hn-n²¹ as the wild type (WT). Ceratopteris spores were surface-sterilized for 5 minutes in a bleach solution, consisting of a 1:3 dilution of bleach (Clorox) and 0.1% Tween 20. The spores were then rinsed three times with sterilized water and spread on Petri dishes of fern medium (FM) containing 0.5 × MS salts and vitamins (PhytoTechnology Laboratories), pH 6.0, and 0.7% (w/v) agar (Sigma-Aldrich). All Ceratopteris spores, gametophytes, young sporophytes, and calli were sealed in plastic bags (Ziploc) to maintain humidity and cultured in growth chambers (Percival) under continuous light at 28°C. After germination, gametophytes remained cultured on FM except for the conditions or experimental settings explicitly described. For the experiment at a lower temperature (Figure S2E), the gametophytes were kept in plastic bags (Ziploc) and cultured under continuous light at room temperature (22°C).

For propagation, individual gametophytes were transferred into each well of 48-well tissue culture plates (Celltreat) containing FM for self-fertilization and the generation of single-spore-derived sporophytes. Young sporophytes were maintained on FM plates for 3-4 weeks and then transferred to propagation media, consisting of half sterile Indiana topsoil and half sunshine #5 propagation mix (Sungro) or half sterile Indiana topsoil and half Propagation Mix BM2 (Berger). Large sporophytes were grown in the LILY greenhouse facility at Purdue under natural light at 28°C for harvesting spores.

FM plates supplemented with Antheridiogen (FM + A_{CE}), which promote the male program, were prepared as follows: her19 spores²⁴ were surface-sterilized as described above and inoculated into FM without agar (100 mg spores/L) in 1- or 2-L flasks. These flasks were shaken on a platform shaker (New Brunswick Scientific, see key resources table) at 110 rpm at 28°C under continuous light in growth chambers (Percival). After 28 days of growth, the suspension culture was filtered to remove gametophytes, and the liquid was recovered for preparing the FM + A_{CE} plates by adding 0.5 × MS salts and vitamins (PhytoTechnology Laboratories), pH 6.0, and 0.7% agar. The efficacy of the FM + A_{CE} plates for inducing male programming was assayed and confirmed using Hn-n spores before the experiments.

METHOD DETAILS

Plasmid construction and plant transformation

The *CrHAM* transcriptional reporter, *pCrHAM::H2B-GFP::3'CrHAM*, was previously described.²² The *CrHAM* translational reporter, *pCrHAM::YPET-CrHAM::3'CrHAM*, was constructed using a similar strategy described previously.^{28,32} The same endogenous 5' promoter and 3' untranslated region/terminator of *CrHAM* were sub-cloned from *pCrHAM::H2B-GFP::3'CrHAM* by restriction enzyme digestion and ligation, and introduced into 5' and 3' end of the *YPET-CrHAM* fragment,²⁸ respectively. The *pCrHAM::Y-PET-CrHAM*::3'CrHAM fragment was then introduced into the pMOA34 vector⁵⁹ for stable transformation.

The *CrHAM RNAi* construct was generated to knock down *CrHAM* in Ceratopteris transgenic lines (as shown in Figure S2A). A 294-bp target fragment was amplified from the *CrHAM* DNA fragment (see Table S2 for primer details) and cloned into the entry vector pCR8 (Invitrogen). The target fragment in pCR8 was then cloned into the pANDA35HK vector⁴³ for stable transformation.

The *CrMIR171B* OE (35S::CrMIR171B) construct was generated to overexpress one Ceratopteris miR171 (CrmiR171b) in Ceratopteris transgenic lines. A 546-bp DNA fragment, which includes the pre-CrMIR171b sequence, was amplified from the genomic DNA of WT Ceratopteris (Hn-n) (see Table S2 for primer details) and cloned into pCR8 through enzyme digestion and ligation. The fragment was subsequently transferred into the pMDC32 vector⁶⁰ for stable transformation.

The constructs were transformed into Ceratopteris Hn-n callus through particle bombardment, following the protocol described previously. 79,80 The plasmid DNA was coated with tungsten microparticles and delivered into Ceratopteris callus through the Bio-Rad Biolistic PDS-1000/He particle delivery system with 1100 psi, as described previously. 79,80 Multiple independent regenerated shoots were selected with hygromycin (Invitrogen, 40 μ g/ml). The spores from each transgenic line were harvested, surface-sterilized, and spread on FM plates containing hygromycin (18 μ g/ml) to test and validate the hygromycin resistance.

For the characterization of the *CrHAM* translational reporter, gametophytes from each independent line were imaged by a ZEISS LSM880 confocal microscope. At least three independent transgenic lines (line 135, line 36, and line 202) were identified, all of which showed comparable expression patterns and levels of the *pCrHAM::YPET-CrHAM::3'CrHAM* reporter in Ceratopteris gametophytes (Figures 1 and S1B). The morphology of these transgenic gametophytes was comparable to that of the WT (Figure S1C). The gametophytes were self-fertilized to produce single-spore-derived sporophytes. The spores of these sporophytes were harvested, and the expression patterns of the reporter were examined again, showing consistent and stable patterns in the gametophytes at the next generation.

Current Biology Article



For the characterization of *CrHAM* KD lines, gametophytes of each independent transgenic line were harvested for quantitative PCR (qPCR) analysis. At least three independent lines (line 37, line 111, and line 251) were identified, displaying a significant reduction in *CrHAM* expression and comparable phenotypes (Figure S2B). For the characterization of *CrMIR171B* OE lines, hermaphroditic gametophytes of each independent transgenic line were harvested for qPCR analysis. Two independent lines (line 5 and line 6) were identified, showing a significant increase in *CrMIR171B* expression and having comparable phenotypes (Figure 7E). Individual gametophytes from each independent *CrHAM* KD line or *CrMIR171B* OE line were self-fertilized to produce sporophytes in the individual wells of the 48-well tissue culture plates (Celltreat). The spores from the single-spore-derived sporophytes were harvested for all the phenotypical characterization in the next generation.

Imaging fluorescent reporters in Ceratopteris gametophytes

The *pCrHAM::H2B-GFP::3'CrHAM* and *pCrHAM::YPET-CrHAM::3'CrHAM* reporters in transgenic gametophytes were imaged using a Zeiss LSM 880 upright confocal microscope (Figures 1 and S1B). Gametophytes at 2-7 DAG were stained with propidium iodide (PI). H2B-GFP was excited using a 488-nm laser line, and the emission was collected from 490-553 nm, as described previously.²² YPET-CrHAM was excited using a 514-nm laser line, and the emission was collected from 508-562 nm. PI was excited using a 561-nm laser line, and the emission was collected from 596-650 nm. Confocal image stacks were processed using Fiji/Image J software⁶¹ to generate z-projection views. Heatmaps of the *pCrHAM::YPET-CrHAM::3'CrHAM* signals (shown in Figure 1) were generated using Fiji/Image J with the Fire selection in the Lookup Tables function.

Quantification of dynamic patterns of YPET-CrHAM

The dynamic patterns of CrHAM protein expressions and accumulation were imaged and quantified, with the aim of correlating them with various functional regions and developmental stages of hermaphrodites and males. Specifically, spores from the *pCrHAM::Y-PET-CrHAM::3'CrHAM* reporter line was surface-sterilized and spread on petri dishes containing FM and 0.7% agar (FM plates). After germination, different gametophytes were randomly sampled each day from 3 DAG to 7 DAG, and the sex type of each sample was defined. Simultaneously, YPET-CrHAM signals from each sample were imaged using confocal microscopy with identical settings. The confocal image stacks were processed using Fiji/Image J software to generate the maximum intensity z-projection view. Different functional regions of the two sex types, including meristems in hermaphrodites, non-meristem regions in hermaphrodites, antheridia in males, and non-antheridia regions in males, were separately partitioned from the projected images using the polygon selections function in Fiji/Image J. The mean signal from each region was quantified using the measure function in Fiji/Image J. To account for background signal, the mean signal measured outside the gametophyte in each projected image was subtracted from the YPET-CrHAM signal in each region. The correlation analysis between the average YPET-CrHAM signal intensity and different functional regions was performed at the indicated DAG (Figure 1T).

Reverse transcription-quantitative polymerase chain reaction (RT-qPCR) analysis

The expression pattern of *CrHAM* (Ceric.08G011800) in WT male and hermaphroditic gametophytes (Figure 1A) was determined by qPCR analysis. Specifically, Ceratopteris WT spores were surface-sterilized and spread on FM plates, and germinated gametophytes were cultured on the same plates. Hermaphrodites and males were separately collected from the same WT population around 7 DAG. Each biological replicate contained the pooled males or hermaphrodites, and three independent biological replicates were included for RNA isolation and qPCR analysis.

Dynamic expression patterns of several genes—*CrGAMYB1* (Ceric.02G004600), *CrGAMYB2* (Ceric.23G083400), *CrGAMYB3* (Ceric.13G080700), *CrCLV1a* (Ceric.11G028700), *CrYUC1* (Ceric.01G116200), and *CrEXP1* (Ceric.05G087800)—were examined at different developmental stages of WT hermaphrodites and males by qPCR (Figures 2O–2R, 5L–5O, S3A–S3D, S3F–S3I, S4G–S4J, and S5H–S5K). Specifically, Ceratopteris WT spores were surface-sterilized and spread on FM plates. At 4, 5, 8, or 10 DAG, hermaphrodites and males were separately collected from the same WT population. Each biological replicate consisted of pooled males or hermaphrodites, and RNA isolation and qPCR analysis were performed with four independent biological replicates. The expression level of *CrGAMYB4* (Ceric.12G025800, one candidate *GAMYB* gene) was also examined in hermaphrodites and males using qPCR, showing no detectable expression during the gametophyte stage (Figure S3N).

Relative expression levels of *CrGAMYB1-3* genes in gametophyte populations of WT and *CrHAM KD* lines were determined (Figures 2S, S3E, and S3J). Specifically, WT and *CrHAM* KD spores were surface-sterilized, spread, and grown on FM plates. All gametophytes, including males and hermaphrodites, were harvested around 7 DAG and pooled as four independent biological replicates for RNA isolation and qPCR analysis.

Relative expression levels of *CrCLV1a*, *CrYUC1*, and *CrGAMYB1-3* during the early developmental stages of the WT and *CrHAM* KD gametophytes were determined by qPCR (Figures 5P, 5Q, and S3K–S3M). Specifically, surface-sterilized Ceratopteris spores were spread on FM plates and cultured under the standard conditions. At 2 DAG, gametophytes from the WT or *CrHAM* KD population were collected for RNA isolation. Simultaneously, other independent 2-DAG gametophytes were supplemented with fresh FM on petri dishes, cultured under the same conditions, and harvested at 3 DAG. Each biological replicate consisted of pooled gametophytes from the WT or *CrHAM* KD, and RNA isolation and qPCR analysis were performed with four independent biological replicates for each genotype at the indicated DAG.

Relative expression levels of CrHAM, CrCLV1a, CrYUC1, and CrEXP1 in hermaphrodites of the WT and CrHAM KD in the absence of exogenous A_{CE} were determined by qPCR (Figures 6E–6G and S2B). WT and CrHAM KD spores were surface-sterilized and grown





individually in wells of 48-well tissue culture plates (Celltreat) containing FM and 0.7% (w/v) agar. This setting eliminated the potential effect of A_{CE} secreted from neighboring hermaphrodites. Hermaphrodites from each well were harvested at 8 DAG and pooled as four independent biological replicates for RNA isolation and qPCR analysis.

Relative expression levels of *CrMIR171B*, *CrHAM*, *CrCLV1a*, and *CrYUC1* were determined in hermaphrodites of WT and *CrMIR171B* OE lines (Figures 7E–7H). Spores of WT, *CrMIR171B* OE line 5 and *CrMIR171B* OE line 6 were surface-sterilized and spread on FM plates. At 5 DAG, hermaphrodites from each genotype were pooled as four independent biological replicates for RNA isolation and qPCR analysis.

All gametophytes used for qPCR were cultured in growth chambers (Percival) under continuous light at 28°C. RNAs were extracted using the RNeasy Mini Kit (Qiagen), and cDNAs were synthesized using the SuperScript Reverse Transcription system (Invitrogen; see key resources table). qPCR was performed using SYBR Green qPCR Master Mix (Selleck Chemicals) on a LightCycler 96 system (Roche) or a CFX duet system (Bio-Rad). *CrACTIN1* served as the reference gene for normalizing gene expression. The qPCR primers for *CrACTIN1*, as previously described, ¹⁶ are listed in Table S2. All other qPCR primers used in this study are also included in Table S2.

Imaging and phenotypic characterization of CrHAM KD lines

Light micrographs of Ceratopteris gametophytes (shown in Figures 2A–2E and S1C) were taken using an Olympus CKX53 microscope with a MIchrome 5 Pro camera and a 10× objective lens. The other gametophytes (shown in Figures 2I–2N, 3B–3I, 4B–4G, 4O–4R, and 4T–4W; Data S1) were stained with PI and imaged using a Zeiss LSM 880 upright confocal microscope with a Plan-Apochromat 10×/0.45 objective lens. PI was excited using a 561-nm laser line, and the emission was collected from 596-650 nm.

The sex ratios in gametophyte populations of the WT or *CrHAM* KD were quantified between 4 and 6 DAG (Figures 2F and 2G) when males and hermaphrodites were morphologically distinguishable. Specifically, WT or *CrHAM KD* spores were surface-sterilized and spread on FM plates in similar density, and germinated gametophytes were cultured under identical conditions. Five independent (1-cm²) squares were randomly selected from FM plates (Figure 2F), and all the gametophytes in each area were stained and imaged by the ZEISS LSM880 confocal microscope. Based on confocal images (as shown in Figures 2I–2N; Data S1), each gametophyte was identified as male or hermaphrodite, and the corresponding sex ratios for each genotype were determined (Figure 2G). The prothallus area of each gametophyte (Figure 2H) was quantified using the Fiji/ Image J software. Similar experiments were performed to quantify the sex ratios in gametophyte populations of the WT and *CrHAM* KD, grown at the standard culture temperature (28°C) and at a lower temperature (22°C) (Figure S2E).

The effects of A_{CE} on hermaphrodite development were quantitatively examined by confocal time-lapse imaging (Figure 3). Specifically, WT or *CrHAM* KD spores were surface-sterilized and grown in individual wells of the 48-well tissue culture plates containing FM and 0.7% (w/v) agar. Gametophytes at 2 DAG were stained with PI and live-imaged by confocal microscopy (Figures 3B–3E). After imaging, gametophytes were rinsed with sterilized water and transferred onto the FM plates supplemented with A_{CE} (FM+ A_{CE}). The same gametophytes were stained with PI and imaged again 4 days after the A_{CE} treatment (Figures 3F–3I). Based on confocal images, each gametophyte was identified as a male or hermaphrodite (Figure 3J), and the numbers of archegonia (the female trait) and antheridia (the male trait) were quantified (Figures 3K and 3L; Table S1).

The single spore assay was performed to quantitatively examine the developmental progress of gametophytes in the absence of exogenous A_{CE} . Each spore was individually inoculated in one well of the 48-well tissue culture plates with lids (Celltreat) containing FM and 0.7% (w/v) agar. Different gametophytes were stained and imaged using confocal microscopy at 2, 3, and 5 DAG, respectively (as representative images shown in Figures 4B-4G). The single spore assay was also performed to determine the sensitivity of the WT and *CrHAM* KD to various concentrations (10%, 50%, and 100%) of exogenous A_{CE} (Figure S2D).

Confocal time-lapse live imaging was performed to determine the cellular dynamics during meristem establishment in WT and CrHAM KD gametophytes (Figures 4O–4R and 4T–4W). Starting from 2 DAG, gametophytes were stained with PI (25 μ g/ml for 2-3 min), rinsed with sterilized water, and imaged on FM plates every 6 hours. Based on previous analysis, time-lapse imaging with the 6-h intervals was sufficient to capture each cell division event. ²² After each imaging session, gametophytes were rinsed with sterilized water a few times, transferred to new FM plates, and cultured in the growth chamber under the same conditions until the next time point.

Confocal image stacks were processed using the Fiji/ Image J software to generate z-projection views. The prothallus area of each gametophyte (shown in Figure 4H) was quantified using the Fiji/ Image J software with Polygon selections and the Measure function based on z-projection views of confocal images. The total cell number of each prothallus (shown in Figure 4I) was quantified using Fiji/ Image J, with each archegonium or antheridium counted as one cell (packet). Computational image analysis (Figures 4S and 4X) was performed as described previously. ^{81,82} The established 2D watershed method for segmentation was described by Vincent and Soille. ⁸³ The MATLAB code used for 2D segmentation and visualization of quantified divison activity is included in Data S7.

Imaging and phenotypic characterization of CrMIR171B OE lines

The sex ratios in gametophyte populations of WT and *CrMIR171B* OE were quantified at 5 DAG (Figure 7). WT or *CrMIR171B* OE spores were surface-sterilized and spread on FM plates at similar density, and germinated gametophytes were cultured under the same conditions. Five independent regions/areas (each measuring 1-cm²) were randomly selected from FM plates (as illustrated in Figure 2F). All gametophytes from these selected areas were analyzed. Specifically, the gametophytes from one selected area for each genotype were stained with PI and imaged using the confocal microscope (as representative images shown in Figures 7K–7P),

Current Biology Article



while the gametophytes from the other four selected areas for each genotype were imaged under the Olympus CKX53 light microscope. Each gametophyte was identified as male or hermaphrodite, and the corresponding sex ratios for each genotype were then determined (Figure 7I). The prothallus area of each gametophyte (Figure 7J) was quantified using the Fiji/ Image J software.

EdU staining and confocal microscopy

The quantitative analysis of S-phase nuclei was performed using the Click-iT Plus EdU (5-ethynyl-2'-deoxyuridine) Alexa Fluor 488 Imaging Kit (ThermoFisher Scientific). WT and CrHAM KD gametophytes were grown individually in single wells containing FM and 0.7% (w/v) agar. 2 DAG gametophytes were soaked with liquid FM supplemented with 10 μ M EdU and cultured under standard growth conditions (continuous light and 28°C) for three hours, followed by an additional hour under vacuum. Samples were then fixed in 3.7% formaldehyde/ 50% (v/v) ethanol/ 5% (v/v) acetic acid (the fixative solution) for 20 min at room temperature. After fixation, samples were rinsed, permeabilized, and labeled with Alexa Fluor 488, following the manufacturer's instructions. Samples were imaged using a Zeiss LSM 880 upright confocal microscope. Alex Fluor 488 was excited with a 488-nm laser line, and the emission was collected from 490-544 nm.

Sequence retrieval and phylogenetic analyses

Arabidopsis R2R3-MYB amino acid sequences were obtained from The Arabidopsis Information Resource (TAIR). R2R3-MYB protein sequences from the ferns *C. richardii* and *Salvinia cucullata* were retrieved from Phytozome 13 and Fernbase (https://fernbase.org/), ^{15,62} respectively, through BLAST with the Arabidopsis R2R3-MYB amino acid sequences as queries. Rice (*Oryza sativa*) R2R3-MYB sequences were obtained from published data. ⁸⁴

CLV1 and EXP homologs were identified via OrthoFinder. ⁶⁴ Amino acid sequences of CLV1/BAM and EXP homologs in the angio-sperms *A. thaliana* and *O. sativa* were retrieved from PLAZA (https://bioinformatics.psb.ugent.be/plaza/). ⁶⁵ Amino acid sequences of CLV1 and EXP homologs in the ferns *C. richardii* and *S. cucullate* were retrieved from Phytozome 13 and Fernbase, ^{15,62} respectively. Amino acid sequences of CLV1 homologs in *M. polymorpha* and *P. patens* were also retrieved from Phytozome 13.

YUC homologs in the ferns *C. richardii* and *S. cucullata* were identified via OrthoFinder⁶⁴ and the related sequences were retrieved from Phytozome 13 and Fernbase, ^{15,62} respectively. Sequences of YUC homologs in *A. thaliana*, *O. sativa*, and *M. polymorpha* were obtained from published data. ^{85–87}

Sequence alignments were performed using MAFFT (version 7) with E-INS-I and default settings. ⁶⁶ The maximum likelihood tree of each gene family (Data S2) was built using IQ-TREE (version 2.2.0). The best-fitting model was selected base on testing with 1000 bootstrap replicates ^{67,88,89} to assess branch support. Phylogenetic trees were visualized and annotated using ITOL (https://itol.embl. de/itol.cgi) ⁶⁸ for presentation.

miR171 sequence analysis

The CrmiR171b and CrmiR171c sequences from *Ceratopteris richardii* were retrieved from Phytozome 13 using BLAST with the Arabidopsis miR171 sequences as queries. Additionally, mature miR171 sequences from 13 land plant species, including *Arabidopsis thaliana*, *Amborella trichopoda*, *Brachypodium distachyon*, *Fragaria vesca*, *Hordeum vulgare*, *Lotus japonicus*, *Oryza sativa*, *Picea abies*, *Pinus densata*, *Physcomitrella patens*, *Pinus taeda*, *Selaginella moellendorffii*, and *Triticum aestivum*, were obtained from miRbase (https://mirbase.org/)⁶³ (listed in Data S6). MicroRNA sequence alignments were conducted using MEGA11⁶⁹ with the default setting of aligning with ClustalW. The secondary structures of CrMIR171b and CrMIR171c were analyzed and predicted through the UNAFold web server (http://www.unafold.org/).⁷⁰

RNA sequencing and analysis

Transcriptome profiling experiments were conducted using RNA-seq to analyze males and hermaphrodites from WT and *CrHAM* KD line 37 (Figures 5A–5I and S4A–S4F). Spores from the WT or *CrHAM* KD line 37 were surface-sterilized and spread on FM plates. At 5 DAG, males and hermaphrodites were separately collected from the same WT population or from the same *CrHAM* KD population. Each biological replicate consisted of pooled males or hermaphrodites, and RNA isolation and RNA-seq analysis were performed with four independent biological replicates (Figures 5A–5I and S4A–S4F). The differential expressions of *CrCLV1a* and *CrYUC1* in hermaphrodites of WT and *CrHAM* KD were also examined by qPCR in these samples (Figures 5J and 5K).

Additionally, RNA-seq experiments were performed to determine transcriptomic changes in hermaphrodites from the WT and *CrHAM* KD in the absence of exogenous antheridiogen (Figures 6A–6D and S5A–S5G). Specifically, spores from the WT or *CrHAM* KD line 37 were individually cultured in wells of 48-well tissue culture plates containing FM and 0.7% (w/v) agar. Hermaphrodites from individual wells were harvested at 8 DAG and pooled as four biological replicates for both the WT and *CrHAM* KD, enabling RNA-seq analysis. Furthermore, the differential expressions of *CrCLV1a*, *CrYUC1*, and *CrEXP1* in hermaphrodites of WT and *CrHAM* KD at 8 DAG were examined by qPCR in an independent batch of samples cultured under the same conditions (Figures 6E–6G).

RNA was extracted using the RNeasy Mini Kit (Qiagen), and RNA quality was assessed by RNA ScreenTape analysis (Agilent). Subsequently, cDNA libraries were prepared by Novogene. These libraries were sequenced on an Illumina NovaSeq platform, generating 150 bp paired-end reads (Novogene). The reads were then mapped to the reference genome of *Ceratopteris richardii* from Phytozome 13 using Hisat2 v2.0.5⁷¹ (Novogene). FeatureCounts v1.5.0-p3 was used to quantify the read numbers mapped to each gene⁷² and FPKM (Fragments Per Kilobase Million) values of each gene were calculated (Novogene). These FPKM values were used for principal component analysis (PCA) and correlation coefficients analysis, performed using the ggplot2 package in R.⁷³





The expression patterns were also visualized and hierarchically clustered in a heatmap plot, illustrating FPKM values (Figure S5A). This was accomplished using the pheatmap R package, ⁷⁴ with the Euclidean distance as the default distance method and complete linkage as the agglomeration method. Furthermore, differentially expressed genes (DEGs) were determined using the DESeq2 R package. ⁷⁵ Specifically, genes with a |fold change| > 2 and an adjusted *P*-value < 0.05 were identified differentially expressed. Volcano plots for DEGs were generated using the ggplot2 R package. ⁷³ Venn plots, illustrating the intersection relationships of different groups of DEGs, were created using the VennDiagram R package. ⁷⁶ Gene Ontology (GO) enrichment analysis of DEGs was performed by the clusterProfiler R package, ⁷⁷ followed by GO slim analysis using the rrvgo R package. ⁷⁸

QUANTIFICATION AND STATISTICAL ANALYSIS

Statistical significance between each pair of two groups was evaluated using the Student's two-tailed t-test in Microsoft Excel (Figures 1A, 3K, 3L, 4H, 4I, 4N, 4Y, 6E-6G, S2B, S2E, and S5D-S5G) or GraphPad Prism (Figures 2O-2S, 5H-5Q, 7E-7H, S3A-S3N, S4G-S4J, and S5H-S5K). For comparison involving multiple data groups, P values were calculated using ordinary one-way ANOVA, followed by Tukey's multiple comparisons test performed with GraphPad Prism (Figures 1T, 2H, and 7J). Values not sharing a common letter indicate significant differences (P < 0.05). Sample size (n), center and dispersion estimation, and significant level for all statistical analysis are described in the figure legends. Differentially expressed genes (DEGs) were determined using the DESeq2 R package. The package of two parts of two properties of two packages are described in the figure legends.

Current Biology, Volume 34

Supplemental Information

A conserved GRAS-domain transcriptional regulator links meristem indeterminacy to sex determination in Ceratopteris gametophytes

Yuan Geng, Chong Xie, An Yan, Xi Yang, Dinh Nhan Lai, Xing Liu, and Yun Zhou

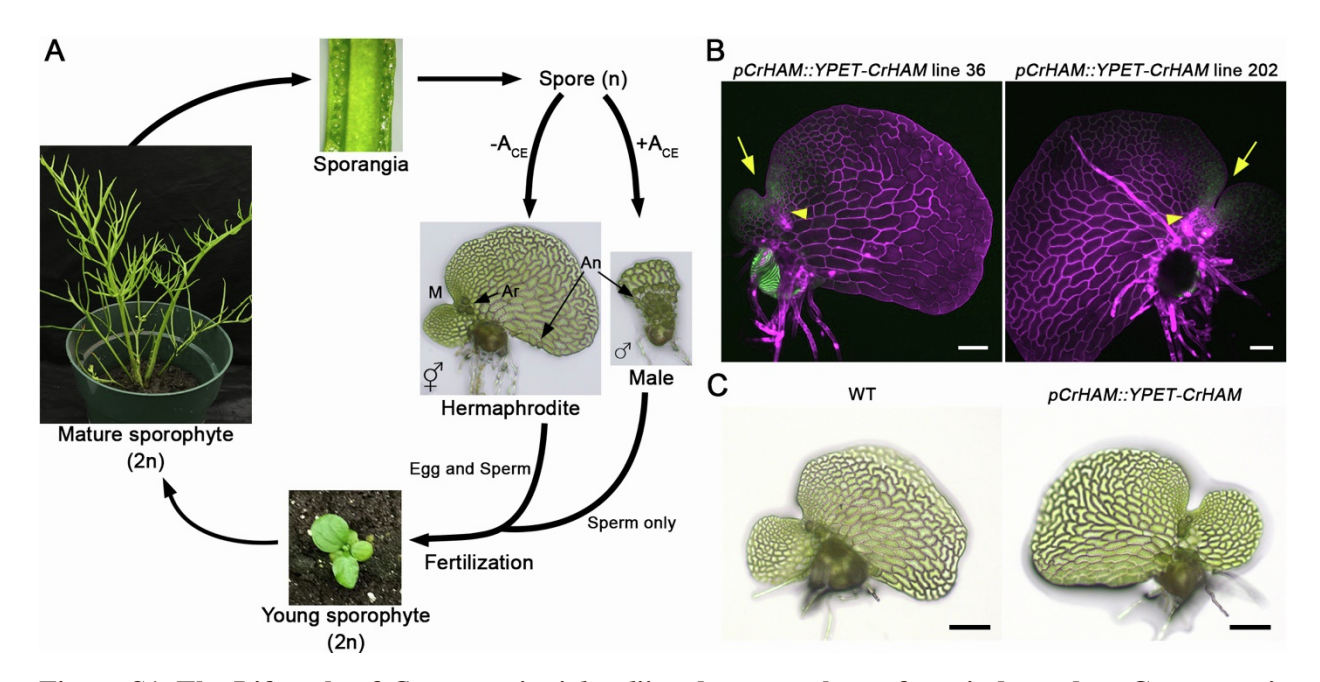


Figure S1. The Lifecycle of Ceratopteris richardii and gametophytes from independent Ceratopteris pCrHAM::YPET-CrHAM transgenic lines. Related to Figure 1. (A) The lifecycle of Ceratopteris richardii. The diploid (2n) sporophyte produces haploid spores (n) via meiosis on the abaxial side of the fronds (in sporangia). Once mature, these spores are dispersed from sporophytes, initiating the gametophyte phase. In the absence of the pheromone antheridiogen (A_{CE}), a haploid spore (n) germinates and develops into a hermaphroditic gametophyte (HG), which forms a meristem (M) and produces both egg-producing archegonia (Ar) and sperm-producing antheridia (An). In the presence of A_{CE}, a spore (n) germinates and develops into a male gametophyte (MG), which lacks a meristem and only produces antheridia. Both hermaphroditic and male gametophytes are free-living and grow independently of sporophytes, Upon reaching sexual maturity, sperm is released from antheridia and swims within archegonia to fertilize an egg, giving rise to a diploid sporophyte (2n) and starting a new life cycle. (B) Hermaphroditic gametophytes of the Ceratopteris pCrHAM::YPET-CrHAM line 36 and line 202 (the other two independent translational reporter lines) were stained with PI and imaged at 5 DAG. Green: YPET-CrHAM: Magenta: PI counterstain. Scale bars: 100 µm. Yellow arrows: meristems; Yellow arrowheads: archegonia. (C) Light micrographs of hermaphroditic gametophytes from the wild-type (WT) control and pCrHAM::YPET-CrHAM reporter line at 5 DAG. Scale bars: 200 um.

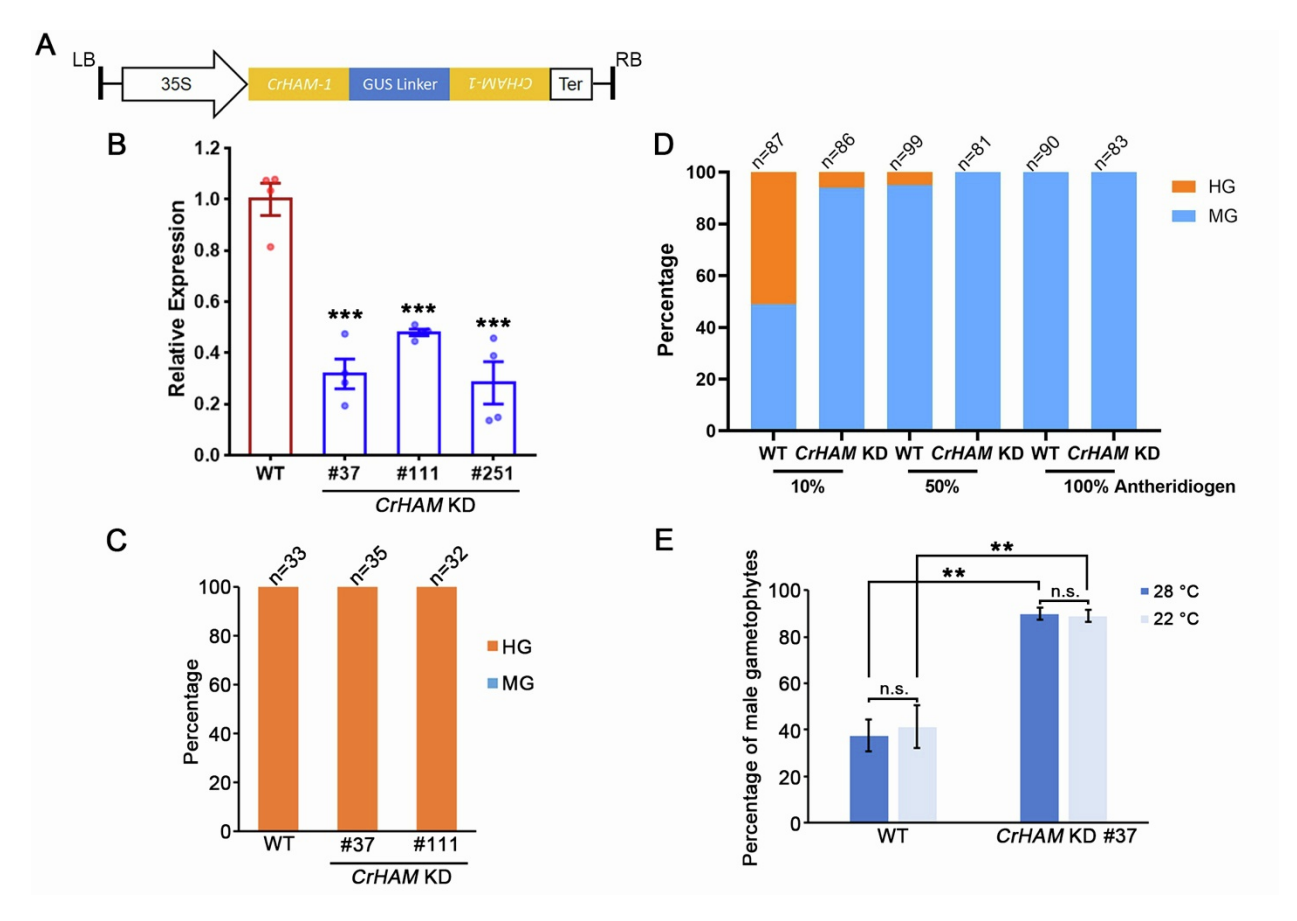


Figure S2. Characterization of CrHAM KD transgenic lines. Related to Figures 2 and 3. (A) A schematic diagram illustrating the CrHAM RNAi hairpin expression cassette in the pANDA35HK binary vector, designed for knocking down the endogenous CrHAM expression. 35S: Cauliflower mosaic virus 35S promoter; CrHAM-1: a 294-bp CrHAM RNAi sequence; Ter: terminator; LB: left border; RB: right border. (B) Relative expression of CrHAM was determined by qPCR analysis and normalized to the expression level of the reference gene CrACTIN1 (CrACT1). Expression levels of CrHAM in CrHAM KD lines were normalized to that of the WT control. Samples included hermaphroditic gametophytes (HG) of the WT control and three independent CrHAM KD lines (37, 111, 251) in Ceratopteris. Bars: means + standard errors of the mean (SEMs), n = 4 biological replicates. ***, P < 0.001 (Student's two-tailed t-test). (C) Percentages of hermaphroditic gametophytes (HG) and male gametophytes (MG) in the WT and CrHAM KD in the absence of exogenous A_{CE}. WT and CrHAM KD spores were sown individually in 48well tissue culture plates containing FM and 0.7% (w/v) agar. The sex type of each gametophyte was determined when males and hermaphrodites were morphologically distinguishable. (D) Percentages of hermaphroditic gametophytes (HG) and male gametophytes (MG) in the WT and CrHAM KD in response to various concentrations of A_{CE}. WT and CrHAM KD spores were sown individually in the 48-well tissue culture plates containing FM, 0.7% (w/v) agar, and different concentrations of A_{CE} (10%, 50%, and 100%). The sex type of each gametophyte was determined when males and hermaphrodites were morphologically distinguishable. (E) Percentages of male gametophytes (MG) in the WT and CrHAM KD populations cultured at different temperatures. Surface-sterilized WT or CrHAM KD spores were spread on FM plates with similar density and cultured under standard growth conditions (high temperature, 28°C) or at a lower temperature (22°C). The sex type of each gametophyte was determined when males and hermaphrodites were morphologically distinguishable. Bars: means \pm SEMs, n=3 biological replicates. Each biological replicate included all gametophytes in one randomly selected area on the petri dishes. n.s.: not significant; **, P < 0.01 (Student's two-tailed *t*-test).

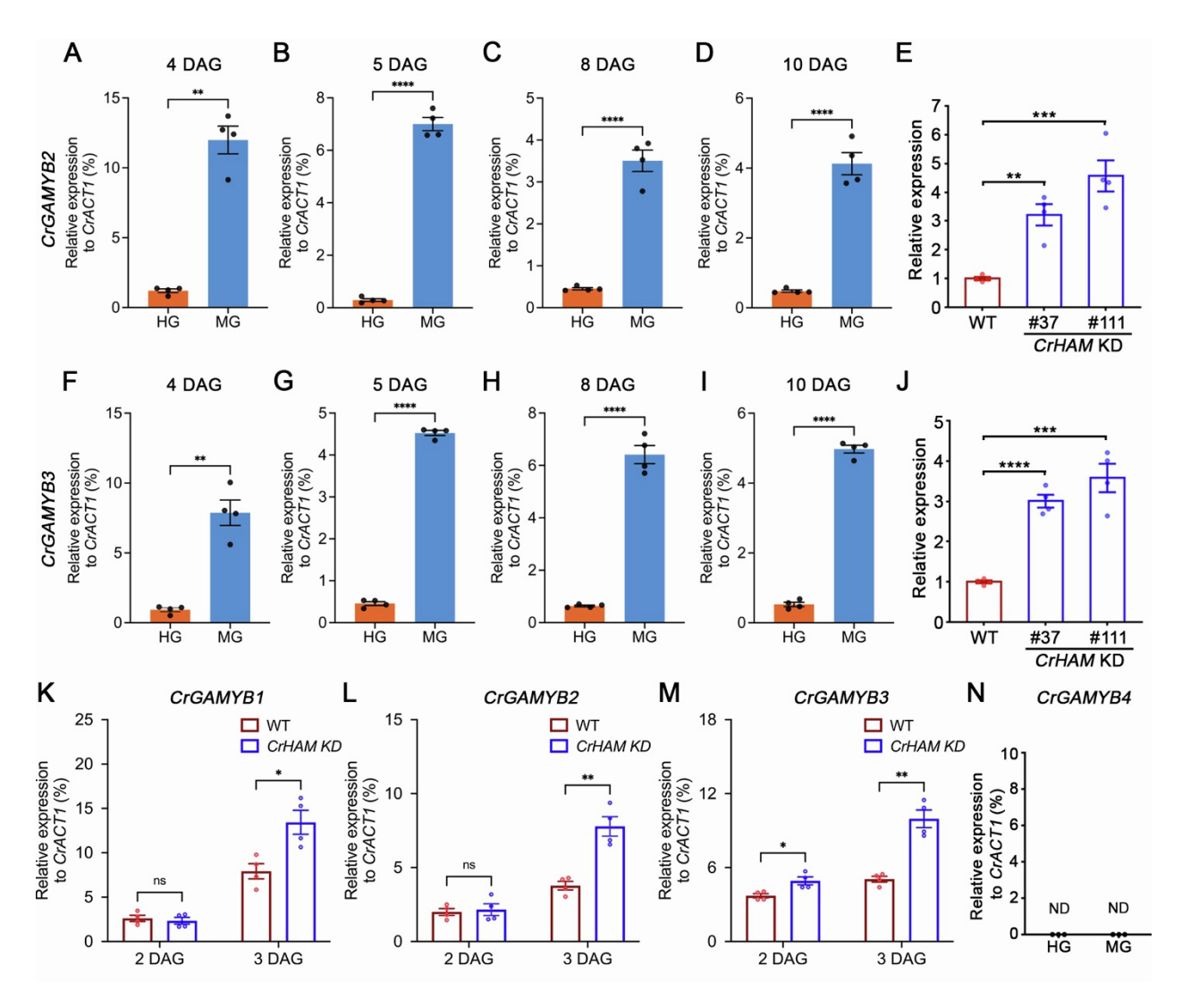


Figure S3. Expression profiles of CrGAMYB **genes in Ceratopteris gametophytes. Related to Figure 2.** (A-D) Relative expression levels of CrGAMYB2 in WT hermaphroditic gametophytes (HG) and male gametophytes (MG) at different developmental stages. (E) Relative expression levels of CrGAMYB2 in gametophytes at 7 DAG from WT and CrHAM KD populations. (F-I) Relative expression levels of CrGAMYB3 in gametophytes at 7 DAG from WT and CrHAM KD populations. (K-M) Relative expression levels of CrGAMYB3 in gametophytes at 7 DAG from WT and CrHAM KD populations. (K-M) Relative expression levels of CrGAMYB1 (k), CrGAMYB2 (l), and CrGAMYB3 (m) in gametophytes at 2 and 3 DAG from WT and CrHAM KD populations. (N) Relative expression levels of CrGAMYB4 in WT HG and MG at 7 DAG. (A-N) Expression levels of CrGAMYB genes were normalized to CrACT1, and in (E, J) the relative expression levels of genes in CrHAM KD were normalized to that in WT. Bars: means \pm SEMs, n = 4 biological replicates. n.s.: not significant. ND: Not detectable. *, P < 0.05; ***, P < 0.01; ****, P < 0.001; ****, P < 0.001 (Student's two-tailed t-test).

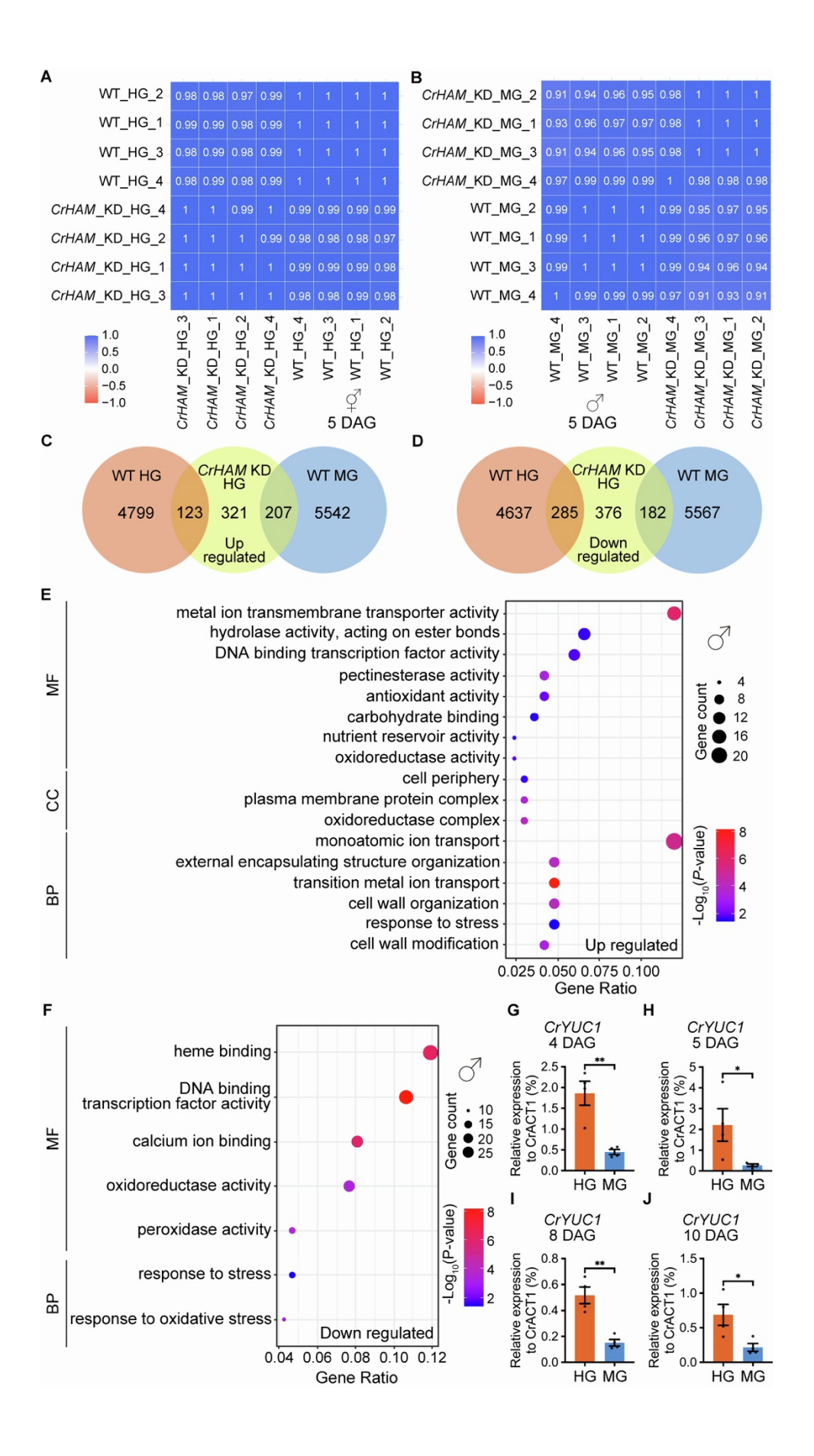


Figure S4. Transcriptomic profiling of males and hermaphrodites in WT and CrHAM KD at 5 **DAG. Related to Figure 5.** (A, B) Pairwise Pearson's correlation coefficient analysis of RNA-seq datasets, including all WT and CrHAM KD samples from either HG (A) or MG (B) at 5 DAG. The correlation coefficient values were color-coded, with darker intensities representing stronger correlation. The numbers on the color blocks represent the calculated correlation coefficients. (C) Venn diagram showing the overlap of up-regulated genes in CrHAM KD HG (yellow, compared to WT HG), HGspecific genes (orange, in WT), and MG-specific genes (blue, in WT). (D) Venn diagram showing the overlap of down-regulated genes in CrHAM KD HG (yellow, compared to WT HG), HG-specific genes (orange, in WT), and MG-specific genes (blue, in WT). (E, F) GO enrichment analysis of up-regulated (E) and down-regulated (F) genes in CrHAM KD MG compared to WT MG. The Y-axis represents enriched GO terms (CC; cellular component; MF; molecular function; BP; biological process). The Xaxis represents the ratios of DEGs annotated to each GO term relative to the total annotated DEGs. Adjusted P-values are color-coded from blue (less significant enrichment) to red (more significant enrichment). Solid circle sizes represent the number of DEGs annotated to each GO term. (G-J) Relative expressions of CrYUC1 at different sex types and various developmental stages were determined by qPCR analysis and normalized to CrACT1. Samples include WT HG and WT MG at 4 (G), 5 (H), 8 (I), and 10 DAG (J). n = 4 biological replicates. Bars: means + SEMs. *, P < 0.05; **, P < 0.01(Student's two-tailed *t*-test).

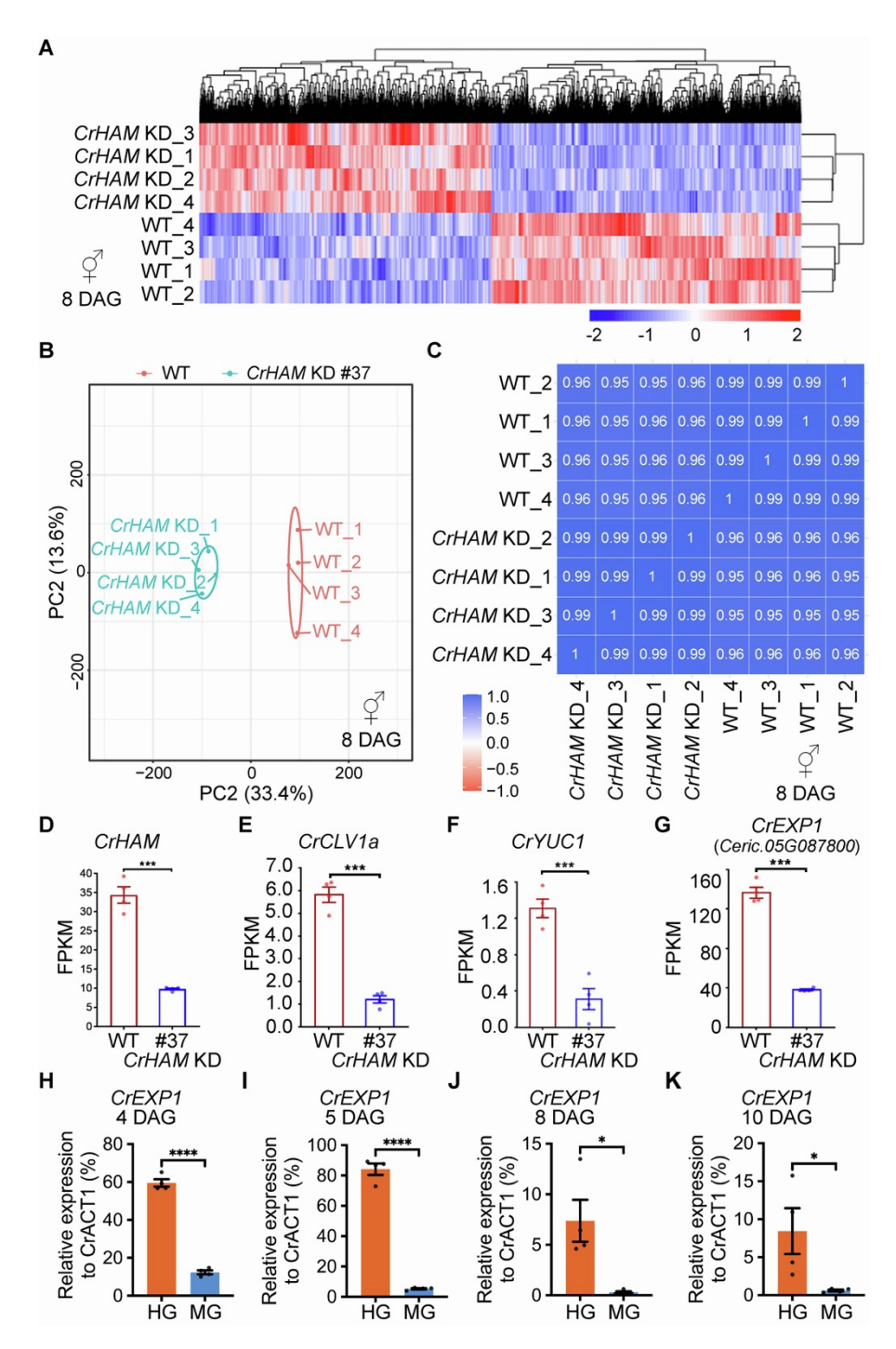


Figure S5. Transcriptomic profiling of hermaphrodites in WT and CrHAM KD at 8 DAG in the absence of A_{CE} . Related to Figure 6. (A) Heatmap illustrating expression patterns in CrHAM KD (line 37) HG compared with WT HG at 8 DAG. Gene expression levels were color-coded from blue (minimum, $\log_2(\text{fold change}) \leq -2$) to red (maximum, $\log_2(\text{fold change}) \geq 2$). Each genotype (WT and CrHAM KD line 37) had four biological replicates. (B) PCA plot of biological replicates for WT and CrHAM KD (line 37) at 8 DAG. Red dots: WT hermaphroditic gametophytes (HG); blue dots: CrHAM KD HG. (C) Pairwise Pearson's correlation coefficient analysis of RNA-seq datasets, including all WT and CrHAM KD samples from HG at 8 DAG. The correlation coefficient values were color-coded, with darker intensities representing stronger correlation. The numbers on the color blocks represent the calculated correlation

coefficients. (D-G) FPKM (Fragments Per Kilobase per Million mapped reads) of CrHAM (D), CrCLV1a (E), CrYUC1 (F), and CrEXP1 (G) at 8 DAG were determined by RNA-seq analysis. Each genotype (WT HG and CrHAM KD line 37 HG) had four biological replicates. Bars: means \pm SEMs. ***, P < 0.001 (Student's two-tailed t-test). (H-K) Relative expressions of CrEXP1 at different sex types and various developmental stages were determined by qPCR analysis and normalized to CrACT1. Samples include WT HG and WT MG at 4 (H), 5 (I), 8 (J), and 10 DAG (K). n = 4 biological replicates. Bars: means \pm SEMs. *, P < 0.05; ***, P < 0.01; ****, P < 0.001; ****, P < 0.001 (Student's two-tailed t-test).